University of Liege – Faculty of Applied Sciences
Aerospace and Mechanical Engineering Department
Thermodynamics Laboratory

Dynamic modeling of a steam Rankine Cycle for concentrated solar power applications

in partial fulfillments of the requirements for the degree of

Engineer in Industrial Technologies

by **ALTÉS BUCH Queralt**

Academic year 2013 – 2014

Abstract

Concentrated solar power (CSP) is expected to play a key role in the necessary energy transition towards more sustainability. However, this type of system is inherently subject to transient boundary conditions such as varying solar irradiation. Therefore, advanced control strategies are required to maintain safe operating conditions and to maximize power generation.

In order to define, implement and test these control strategies, dynamic models of the system must be developed. This thesis aims at developing a model of a steam Rankine Cycle coupled to a field of parabolic troughs.

The modeled system does not correspond to an existing plant, but its characteristics are defined as realistically as possible with information coming from different sources. Simplified but also physical, lumped dynamic models of each component (boiler, turbines, condenser, solar collectors) have been developed and parametrized using the ThermoCycle library, written in the Modelica language. These models have been further interconnected to build the CSP plant model, whose response has been tested to fluctuating atmospheric conditions.

The proposed library of models is based on an innovative lumped-parameter approach aiming at developing physical models that are significantly more robust and computationally efficient than the traditional libraries of models already available. The final purpose of these models is high level simulations (e.g. for control purposes), but not the modeling of detailed physical phenomena.

The different models have been successfully tested with the example of the CSP plant, but can also be applied in other fields of thermal engineering. They proved to be more robust and much faster than the traditional models, which was the objective. However, in the scope of this work, it has not been possible to validate them with experimental data or with more detailed models. This should be the priority for future works.

Acknowledgements

I am very grateful to Dr. Sylvain Quoilin, who made this work possible. I wish to thank him for his countless advises and permanent availability, which have been essential for this work.

I would like to thank some members of the laboratory, namely I. Bell, S. Bellolio, A. Desideri, R. Ruiz and K. Sartor, for their interesting discussions and their help in many occasions.

I am also grateful to Professor Pierre Dewallef, for his advises and explanations, as well as for providing me helpful data for the development of the work.

A special thanks goes to all the members of the thermodynamics laboratory, who warmly welcomed me, and provided an excellent atmosphere. The last six months have been priceless in a personal level.

Last but not least, I would like to thank my family and friends for their unwavering support, even in the distance.

Table of contents

Abstract 2
Acknowledgements 3
Table of contents 4
Nomenclature 6
1 Introduction 8
1.1 Dynamic Modeling of CSP systems and steam cycles: state of the art 8
1.2 Goal of this work 11
2 Combined heat and power (CHP) plant of Sart-Tilman 14
3 Modeling 17
3.1 Previously available models 19
3.1.1 Finite Volume models 19
3.1.2 Pump 20
3.1.3 Heat exchanger 22
3.1.4 Pressure drop 23
3.1.5 Tank 24
3.1.6 Solar field 26
3.2 Models developed in the scope of this thesis 29
3.2.1 Stodola steam turbine 29
3.2.2 Cross-flow condenser 31
3.2.3 Thermal resistance 34
3.2.4 Linear valve 35
3.2.5 Two-phase drum 37
3.2.6 Heat exchangers 41
3.2.7 Closed volume 49
3.2.8 Saturation state sensor 50

3.2.9 Base components with (p,T) as state variables 50
4 CSP plant model 54
4.1 Boiler system 54
4.2 Overall cycle model 58
4.3 Thermo-physical properties of the working fluids 66
4.3.1 Integration of the thermo-physical properties: TTSE method 66
4.3.2 Avoiding chattering and flow-reversals: density smoothing 67
4.3.3 Incompressible fluids 68
5 Control of the plant 69
6 Simulation results 71
6.1 Simulation 1: Varying the DNI 73
6.2 Simulation 2: Varying the working fluid flow rate in the preheater 75
6.3 Simulation 3: Changing the position of the steam extraction 77
6.4 Simulation 4: Varying the mass flow rate in the evaporator 78
7 Conclusions and perspectives 81
Bibliography 84

Nomenclature

A	area, m^2	N	number of cells, –
AU	heat transfer conductance, W/K	n	number of tubes, –
c_p	specific heat capacity, J/kgK	p	pressure, bar or Pa
D	tube diameter, mm or m	$\dot{Q}$	heat power, W
e	error, –	r_p	pressure ratio, –
f	frequency, Hz	T	temperature, ºC or K
H	enthalpy, J	t	thickness, mm
h	specific enthalpy, J/kg	t	time, s
K	coefficient of Stodola's law, –	U	heat transfer coefficient, W/m^2K
K_p	proportional gain, –	U	internal energy, J
L	pipe length, mm or m	V	volume, m^3
L	tank relative level, –	$\dot{V}$	volume flow rate, m^3/s
M	mass, kg	x	vapor quality, –
$\dot{M}$	mass flow rate, kg/s	$\dot{W}$	power, W

Greek Symbols

ε_v	volumetric effectiveness, –	ε	parameter *LMTD_robust*, –
τ_I	integral time, –	η	efficiency, –
Δ	differential	ξ	penalty factor, –
ε	effectiveness, –	ρ	density, kg/m^3

Subscripts and Superscripts

*	adjacent cell index	i	internal
0	initial (when t=0)	iso	isothermal
cf	cold fluid	l	liquid
eco	economizer	max	maximum
eva	evaporator	nom	nominal
ex	exhaust	o	external
hf	hot fluid	sf	secondary fluid
i	cell index	sh1	first superheater

sh2	second superheater
su	supply
tube	tube
v	vapor
w	wall
wf	working fluid

Acronyms

CFD	Computational Fluid Dynamics
CHP	Combined Heat and Power
CSP	Concentrated Solar Power
DHN	District Heating Network
DNI	Direct Normal Irradiation
EES	Engineering Equation Solver
EOS	Equation Of State
HCE	Heat Collector Element
HPT	High Pressure Turbine
HTF	Heat Transfer Fluid
IEA	International Energy Agency
LMTD	Log Mean Temperature Difference
LPT	Low Pressure Turbine
PV	Photovoltaic Systems
SEGS	Solar Electric Generating Systems

Chapter 1

Introduction

1.1 Dynamic Modeling of CSP systems and steam cycles: state of the art

The Concentrated Solar Power (CSP) technology provides an alternative to photovoltaic (PV) systems for clean power generation. According to the IEA (International Energy Agency, 2010), CSP also presents a strong potential to be a key technology to address climate change, because of its very low levels of greenhouse-gas emissions. Furthermore, CSP has an inherent capacity to store thermal energy for short periods of time, which can be later converted to electricity. This is an important feature at a time where flexibility of power plants is getting more and more importance, e.g. to participate to the reserve electricity markets. Finally, thermal storage capacity combined with CSP plants allows producing electricity even on a cloudy or foggy day or after sundown.

Nowadays, it is estimated that the total CSP global capacity is about 2550 MW (Renewable Energy Policy Network for the 21st Century, 2013). The CSP market has doubled between 2011 and 2013, with Spain leading for both deployment and total capacity accounting for 1950 MW. According to (International Energy Agency, 2011) analysis: *under extreme assumptions solar energy could provide up to one-third of the world's energy demand after 2060*.

There are three main types of CSP power plant (Quoilin, 2007):

- **Parabolic trough**: this type of plant is the most used solar technology because of its technological maturity (the first plants were installed in the 80's) and its investment and operating costs. It has the best land-use factor and other advantages (e.g. storage capability, lowest materials demand, modularity and hybrid concept proven). The main installation is made of a solar field, a heat exchange system and an electrical generation system. The collectors are formed by a parabolic trough reflector (mirror), a metal structure, a receptor pipe and the following solar system. The metal tube, which is placed inside a

vacuum glass envelope, runs the length of the trough at its focal line and absorbs the thermal energy that the collector receives. The fluid (synthetic oil) that flows inside is therefore heated up to approximately 300-400ºC and is then pumped to traditional heat exchangers in order to produce the steam that will run a turbine and an electric generator.

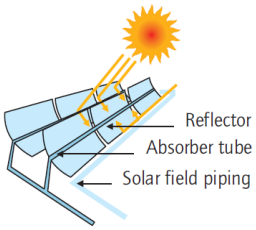

Figure 1 (International Energy Agency, 2010)

- **Parabolic dish**: this type of technology works in an autonomous way (i.e. they can be installed in isolated places, with no electrical connections) and presents a relatively high conversion efficiency (over 30%). It is made of a reflective parabolic surface with two axes that follows the sun and concentrates the solar rays to the focus of the parabola. The concentration factor can be higher than 2000, leading to a temperature of 750ºC. Hybrid operation is possible. However, its reliability should be improved.

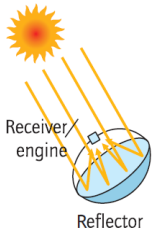

Figure 2 (International Energy Agency, 2010)

- **Solar tower**: this type of plant is formed by many flat, movable mirrors (called heliostats) that focus the sun's rays upon a boiler placed at the top of a tower. It has less ambient losses than parabolic troughs because the exposed surface is limited. The concentration factor varies from 600 to some thousands, allowing reaching temperatures from 800ºC to 1000ºC. Storage can be used at high temperatures and there is also the possibility of hybrid operation.

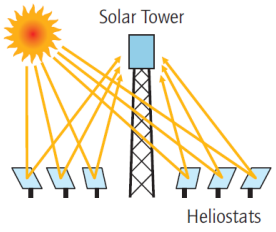

Figure 3 (International Energy Agency, 2010)

This work focuses on the parabolic trough technology, because it is by far the more widespread and the one with the highest commercial maturity (SolarPACES, 2014).

Moreover, it allows decentralized power generation and low collector temperature (Quoilin et al., 2011a), which widens it range of applicability.

Because of the wide range of atmospheric conditions (mainly irradiation level and temperature) in which these systems can be installed, it is very useful to develop thermodynamic models of CSP systems. Steady-state models are useful for sizing problems, system performance evaluation or cycle optimization problems. They can be used in very different conditions and can for example help evaluating the system performance in a particular location. Nevertheless, they cannot be used to evaluate the cycle performance under highly transient conditions, nor can they be utilized for defining a proper control strategy.

On the other hand, dynamic models are defined for transient conditions. They are suitable for dynamic control issues, dynamic phenomena such as start or shutting down, or to estimate the cycle performance under transient heat source conditions. They are therefore very important in solar power systems, in which the nature of the solar source is discontinuous (i.e., transient boundary conditions). Since thermal energy storage is involved, proper dynamic simulations are required to evaluate and optimize their response time as well as test control strategies.

Dynamic models of CSP systems, and in particular of parabolic troughs, are scarce in the scientific literature. (Forristall, 2003) proposed a steady-state heat transfer model implemented in Engineering Equation Solver (EES) validated with monitoring data from the solar electric generating systems (SEGS) in California.

(Manenti and Ravaghi-Ardebili, 2013) present a dynamic model of a CSP plant based on a commercial simulation package. The CSP unit is made of parabolic trough collectors with a two-tanks direct heat storage. (Powell and Edgar, 2012) study the same type of plant, but only focus on the solar loop without considering the power block. A simple control strategy is developed to maintain a constant heat transfer through the boiler.

(Llorente García et al., 2011) present a detailed performance model for a parabolic trough plant with a two-tanks *indirect* heat storage. The model results are compared to actual experimental data, with which a good agreement is found. The importance of modeling start-up and shut-down procedures considering their frequency in such technology is emphasized. However, because of the difficulty to simulate null flow rates (see for example (Espinosa et al., 2011)), it has not been fully performed.

(Bonilla et al., 2011) developed a model of direct steam evaporation inside the troughs, focusing on the difficulty to handle phase transitions inside of a single evaporation tube.

Most of the above models focus only on the solar system (with or without storage). The power plants are usually not modeled in details. However, the dynamic modeling of steam power plants has been the object of largeliterature (Casella and Leva, 2003; Colonna and Van der Stelt, 2004; Fritzson, 2010; Jensen, 2003; Quoilin et al., 2011b; Tummescheit, 2002; Tummescheit et al., 2000). It appears that, when modeling thermo-flow problems, the Modelica language is well suited due to its a-casual formulation allows connecting the models in a physical way (Casella et al., 2007). A number of libraries have been developed in this language: ThermoSysPro, Power Plants, Thermal Power, ThermoPower, ThermoCycle, etc. However, very few models are freely available:

- The ThermoPower library contains several models of gas turbines, steam and combined cycle power plants. Some components of the cycle are simplistic (e.g. the condenser is modeled by a prescribed pressure), whereas the heat exchangers in the boiler are modeled using a finite volumes approach.
- The ThermoSysPro library, developed by EDF is freely available upon request. It aims at modeling complex power plants for control purposes. The main drawback is its lack of compatibility with the Modelica Standard Library and the difficult re-usability of its models.
- The ThermoCycle library was originally designed for small-scale thermodynamic systems (e.g. heat pumps and Organic Rankine Cycles). It does not comprise any model of a whole steam power plant.

All the above models rely on the 1D finite volume formulations for the computation of fluid flows and heat transfer. However in dynamic modeling, finite volume flow models, especially those involving two-phase flow, are subject to several numerical issues, which decrease the simulation speed and potentially lead to simulation failures. In (Quoilin et al., 2014a) different heuristic strategies are presented to tackle numerical problems while improving the robustness. However these methods do not provide a fully reliable solution regarding the robustness, and do not improve the simulation speed.

1.2 Goal of this work

This thesis aims at developing a detailed model of a steam Rankine cycle under transient conditions coupled to a parabolic troughs field. Due to the lack of information, the modeled system does not correspond to an existing plant, but its characteristics are defined as realistically as possible with information coming from different sources:

- The solar field characteristics are taken from well-known CSP plants in California through a validated model (Forristall, 2003) translated into the Modelica language
- The steam plant characteristics are based on a real test case: the biomass Combined Heat and Power (CHP) plant from the university campus at Sart-Tilman (Belgium). However, since this plant is originally a biomass plant and not a solar plant, significant modifications must be brought to the boiler design. The CHP possibility (i.e. a second, higher-temperature condenser) is also removed.
- No heat storage is considered in the scope of this thesis

In order to achieve the main goal, proper dynamic models of the components of the cycle must be developed, with the need of being robust as well as computationally efficient. These models will be included in the ThermoCycle library, an open-source Modelica library for the modeling of thermal systems, so they can be re-used afterwards.

By contrast to the dynamic models developed in most previous works, this thesis aims at developing simplified but also physical, lumped models of each component. As an example, most models (previously described in section 1.1) make use of the traditional finite volume approach to model heat exchangers, e.g. 3D-discretized models known as Computational Fluid Dynamics (CFD) models, or more simplified but still complex 1D-discretized models such as those available in the ThermoPower library. However, this approach involves many thermodynamic property calls and multiplies the number of nonlinear equations (at least one per cell or node). Therefore, these models are not very robust (i.e. the convergence of the Newton Solver is not ensured), and are computationally-intensive. Provided some hypotheses are met, these models could be advantageously replaced by lumped dynamic models, e.g. using the LMTD method. Such an approach is appropriate for the following:

- The level of details required by the simulation is low: its main goal is the evaluation of the heat exchanger behaviour integrated in a wider system, rather than the accurate computation of the heat transfer and pressure drop. This is especially the case when implementing and testing control strategies of a whole system or power plant.
- Few information is available on the exact geometry of the heat exchangers. In this case, a lumped approach should be as good as a detailed model, provided that the main physical phenomena are taken into account.

As an example, the whole heat transfer phenomena involved in an evaporator, which is quite complex due to the special variability of its main thermo-flow characteristics (fluid velocity, heat transfer coefficient, etc.), would be modeled by means of the ε-NTU method taking into account some hypotheses. This leads to one simply equation

with some assumptions, such as a constant, lumped thermal conductance (AU). This approach dramatically simplifies the physical model, and therefore increases its robustness and computational efficiency. In this thesis, this kind of model will be referred to as semi-empirical or lumped parameter dynamic models, as a tradeoff between purely empirical models and deterministic finite volumes models. It should be noted that, in most cases, the semi-empirical models require experimental data or at least a nominal operating point so their parameters can be tuned.

In summary, **the main goal of this thesis is to propose a simplified, but still physically meaningful set of semi-empirical dynamic models describing the main components of a parabolic trough CSP plant.** After the development of each subcomponent model, a dynamic model of the overall cycle is built for the purpose of evaluating the system's reaction to transient conditions. The model consists in a parabolic trough model coupled to a steam cycle model.

Chapter 2

Combined heat and power (CHP) plant of Sart-Tilman

In order to provide realistic parameters to the dynamic model of the steam Rankine cycle, the latter is based on the biomass-CHP plant available in the Sart-Tilman Campus. This plant is an extraction-condensing CHP plant connected to a district heating network of the University campus (Liège, Belgium). The cycle layout and the main components are assumed to be similar for a biomass-fired system as for a CSP system, at the exception of the boiler since the heat source characteristics are different (high temperature flues gases vs. medium-temperature thermal oil).

Figure 4: CHP plant of Sart-Tilman (Granulenergie, 2014)

In the considered CHP plant, the District Heating Network (DHN) distributes pressurized hot water at 125 ºC trough a total length of 10 km to approximately 70 buildings, representing a total heated area of about 470 000 m^2. Classrooms, administrative offices, research centers, laboratories and a hospital are the main installations of these buildings. The effective peak power of the network is around 56 MWth for a total of 60 000 MWh per year (Sartor et al., 2014). It should however be noted that the CHP system only provides a small fraction of this thermal energy, the remaining being ensured by gas-fired boilers.

The plant consists of a biomass furnace connected to a boiler made of an economizer, an evaporator and a superheater section. The live steam is expanded in a back-

pressure turbine after which a portion of the steam is extracted and condensed to supply the heat to the district heating network. The remaining steam is sent to a condensing turbine and passes through a condenser before returning to the deaerator (Sartor et al., 2014).

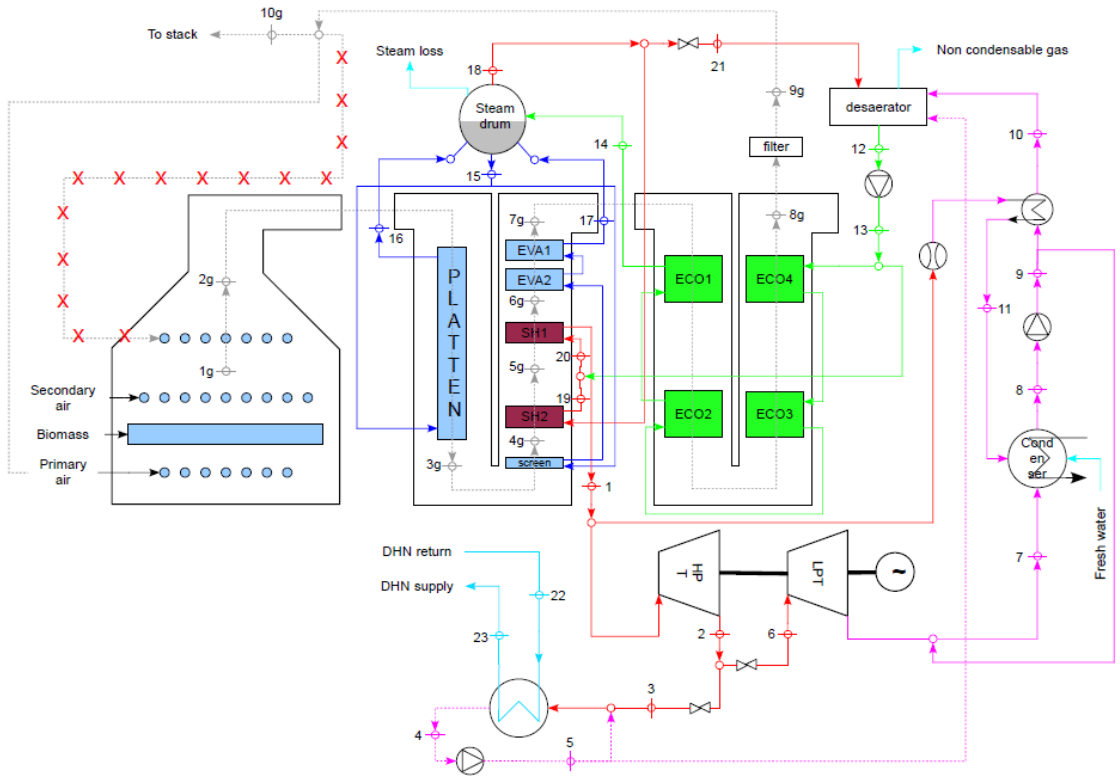

Figure 5: Schematic of CHP plant (Sartor et al., 2014)

Nevertheless, it should be stated that this work is not focused on modeling this plant but in using it to have realistic parameters to design a steam Rankine cycle in order to couple it to a field of parabolic troughs. Furthermore, considering that the real plant is a cogeneration CHP plant, the DHN part will not be taken into account, i.e. there will be no steam extraction after the high pressure turbine to supply it.

The main known characteristics of the plant are:

Heat source	Composition: 10,73% CO_2, 14,93% H_2O, 67,54% N_2, 6,73% O_2, 0,07% SO_2		
Condenser	U-tube cross-flow condenser	n = 876 tubes	$\dot{Q}_{nom}$ = 8 132 kW
	$D_{i,tube}$ = 22,90 mm $D_{o,tube}$ = 25,40 mm t_{tube} = 1,25 mm L = 4 000 mm	**Shell Side** Steam x_{nom} = 0,886 $\dot{M}_{nom}$ = 14 000 kg/h T_{nom} = 58,5 ºC	**Tube Side** Propylene glycol 40% $\dot{M}_{nom}$ = 515 176 kg/h Heated from 34,5 to 49,5 ºC

HPT	$P_1 \in [39 ; 43]$ bar $T_1 \in [380 ; 420]$ ºC	P_2 = 5,4 bar $T_{2,\,max}$ = 347 ºC	$P_{1,nom}$ = 41 bar
LPT	$P_6 \in [4{,}4 ; 6{,}8]$ bar $T_6 \in [164 ; 347]$ ºC	$P_7 \in [0 ; 1{,}2]$ bar $T_{7,\,max}$ = 304 ºC	$P_{6,nom}$ = 5,3 bar $P_{7,nom}$ = 0,16 bar
Deaerator	V = 14 m^3		
Boiler	$\dot{Q}$ = 9 454 kW		
DHN condenser	$\dot{Q}$ = 3 641 kW		
Steam cycle	$\eta_{electrical}$ = 16,03 %	$\dot{W}_{electrical}$ = 1 685 kW	$\eta_{overall}$ = 16,03 %

Table 1 (Source: ARI, 2014)

As shown in the table above, very few data of the cycle is available. A simplified steady-state model of the system previously developed in (Sartor et al., 2014) has been very helpful to set the system nominal conditions and to define the start values for the initialization part of the simulation.

Chapter 3
Modeling

This section describes the dynamic modeling of different components involved in the steam Rankine cycle (both for CHP and CSP applications) and in the parabolic troughs solar field. The models are implemented in the Modelica language and the fluid properties are computed in CoolProp.

Components in most thermodynamic systems are interacting with each other, which usually lead to implicit equation systems. The equations and connections in Modelica are acausal. Acausal modeling is the concept of stating the model equations in a neutral form without considering the computational order. Furthermore, it is closely connected to physical modeling (i.e., the concept of building system models by connecting component models reflecting the physical structure of the system) (Jensen, 2003).

The process of solving a dynamic system simulation is divided into two consecutive steps: the *initialization* and the *simulation* phase. The first one assigns coherent values to all the model variables, which are used for the initial step (t=0), and the latter computes a trajectory (Quoilin, 2011).

Some of the models used for the dynamic modeling of the cycle were previously available in ThermoCycle, an open-source Modelica library for the modeling of thermal systems:

- **Pump** (*pump*): lumped model based on performance curves in which the pump speed is set as an input.
- **Heat Exchanger** (*hX1DInc*): counter-current plate heat exchanger in which one of the two fluids is modeled as an incompressible fluid.
- **Pressure drop** (*dp*): lumped model that computes a punctual pressure drop.
- **Two-phase tank** (*tank_pL*): fully-mixed two-phase tank model with pressure and level as state variables.
- **Solar field** (*SolarField_Forristal_Inc*): dynamic model based on the steady-state (Forristall, 2003) model.

Nonetheless, most of the models used are new models that have been built for the purpose of this work. The developed models are intended to be very simple (as explained in section 1.2), in order to maximize the robustness and the rapidity of the simulation. Therefore, most of them are non discretized models, with some simplifications but also some dynamics. The developed models are:

- **Stodola Steam Turbine** (*steamTurbine*): steam turbine modeled by Stodola's elliptic law (based on the steam turbine from the ThermoPower library), but with some modifications and options that increase the robustness of the model.
- **Cross-flow Condenser** (*crossCondenser*): water-cooled condenser modeled as a cross-flow heat exchanger in which the secondary fluid is discretized and modeled as an incompressible fluid.
- **Thermal Resistance** (*thermalResistance, thermalResistanceL*): discretized and non-discretized models of a thermal resistance between two temperature profiles.
- **Linear valve** (*valve_lin*): lumped valve model assuming a linear relationship between the mass flow rate and the pressure drop
- **Two-phase drum** (*drum_pL*): fully-mixed two-phase drum model with one inlet and two outlets (i.e. liquid and vapor), and with pressure and relative level as state variables. Two specific components for the steam cycle derivate from it:
  - **Boiler drum** (*boiler_drum*): is the drum in the boiler system.
  - **Deaerator** (*deaerator*): is the deaerator of the steam cycle.
- **Heat exchangers:** non-discretized counter-current heat exchangers
  - **Single-phase** (*HX_singlephase_pT*): both working and secondary fluids are single-phase and are modeled based on the LMTD method but with some dynamics:
    - Function LMTD_robust: modified version of the LMTD method that is more robust and computationally efficient for dynamic modeling.
  - **Two-phase** (*HX_twophase_pT*): the working fluid (cold) is in a two-phase state, the wall is assumed isothermal, and the secondary fluid (single-phase) is modeled by:
    - Semi isothermal heat exchanger (*Semi_isothermal_Heat_Exchanger _pT*): models the heat exchange between a fluid and an isothermal wall by means of the ε-NTU method.
- **Closed Volume** (*volume*): closed volume of working fluid with a possible heat exchange, which acts as a mass damper (i.e. absorbs or rejects part of the flow).
- **Saturation state Sensor** (*sensSat*): saturation state sensor for two-phase flows that outputs the saturation temperature, pressure and vapor quality.
- **Base components with (p,T) as state variables**
  - Connector flange (*flange_pT*, *flangeA_pT*, *flangeB_pT*): stream connector for single-phase flows.

- Flow rate source (*sourceMdot_pT*): ideal mass flow rate source for single phase flows.
- Pressure sink (*sinkP_pT*): for single phase flows.
- Flange converter (*flangeConverter*): between (p,h) and (p,T) connectors.

3.1 Previously available models

3.1.1 Finite Volume models

Dynamic modeling of heat exchangers can be classified in two main categories (Quoilin, 2011):

- Moving boundaries: in which there are several zones, whose boundaries vary in time according to the current conditions.
- Discretized models: known as finite volume models, in which the 1D flow is subdivided into several equal control volumes.

Although finite volume models are slower than moving boundaries models (Bendapudi et al., 2008), they are more robust through start-up and load-change transients.

Some models already available in ThermoCycle and used in this work (e.g. *Hx1DInc*) are developed using the finite volumes approach. In these models, the flow is discretized into N cells in which the energy and mass balance are applied (the momentum balance is neglected). The fluid properties are assumed to vary only in the flow direction.

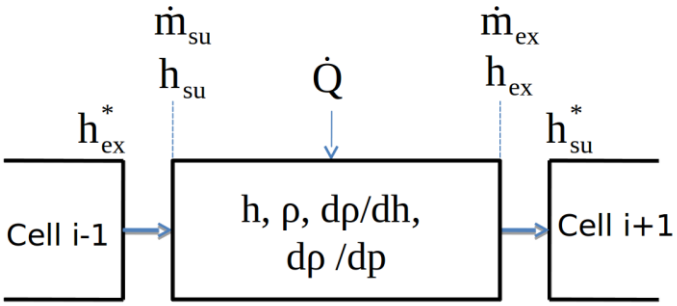

Figure 6: Discretized flow model with cells and node variables (Quoilin et al., 2014a)

As shown in Figure 6, both node (i.e. with subscripts "su"–supply and "ex"–exhaust) and cells variables (i.e. without subscripts) are defined for each cell and the adjacent ones (distinguished by the the "*" exponent). For a compressible flow with (p, h) as differentiated state variables, the mass balance is written (Quoilin, 2011):

$$\dot{M}_{su} - \dot{M}_{ex} = V_i \cdot \frac{d\rho}{dt} = V_i \cdot \left(\frac{\partial \rho}{\partial h} \cdot \frac{dh}{dt} + \frac{\partial \rho}{\partial p} \cdot \frac{dp}{dt} \right) \quad (1)$$

where $\frac{\partial \rho}{\partial h}$ and $\frac{\partial \rho}{\partial p}$ are considered as thermodynamic properties of the working fluid and are computed in CoolProp.

For each cell, the energy balance is written:

$$\frac{dU_i}{dt} = \dot{M}_{su} \cdot h_{su} - \dot{M}_{ex} \cdot h_{ex} + \dot{Q}_i + \dot{W}_i - p \cdot \frac{dV_i}{dt} \quad (2)$$

where $\dot{Q}_i$ is the heat flow to the cell. Recognizing that $U_i = H_i - p \cdot V_i$ and that the internal work $\dot{W}_i$ is null, the equation becomes:

$$V_i \cdot \frac{d\rho_i}{dt} \cdot h_i + V_i \cdot \rho_i \cdot \frac{dh_i}{dt} - V_i \cdot \frac{dp}{dt} = \dot{M}_{su} \cdot h_{su} - \dot{M}_{ex} \cdot h_{ex} + \dot{Q}_i \quad (3)$$

Combining (1) and (3), the energy balance is finally written (Quoilin, 2011):

$$V_i \cdot \rho_i \cdot \frac{dh_i}{dt} = \dot{M}_{su} \cdot (h_{su} - h_i) - \dot{M}_{ex} \cdot (h_{ex} - h_i) + \dot{Q}_i + V_i \cdot \frac{dp}{dt} \quad (4)$$

In the case of incompressible flows, it is considered that the inlet and outlet flow rates are equal (the thermal expansion is neglected). The mass balance equation is therefore not necessary and the energy conservation equation (3) simplifies into:

$$V_i \cdot \rho_i \cdot \frac{dh_i}{dt} = \dot{M} \cdot (h_{su} - h_{ex}) + \dot{Q}_i \quad (5)$$

When interconnecting several cells in series, the relation between the cell and node variables is defined by the discretization scheme. In (Quoilin et al., 2014a) two schemes were presented, both implemented in the ThermoCycle library:

- The central difference scheme: $h = (h_{su} + h_{ex})/2$
- The upwind scheme: $h_{ex} = h$

where h_{su} and h_{ex} are expressed differently in both schemes and depend on the direction of the mass flow rate. The discretization scheme selected in this work is the upwind scheme because of its higher robustness.

3.1.2 Pump

The *Pump* model computes the compression of a fluid in a turbo or volumetric machine. It is a lumped model based on performance curves, in which the pump speed is set as an input.

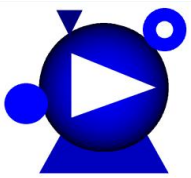

Figure 7: Icon of the *pump* model

The main assumptions for this model are:

- No dynamics (considered negligible when compared to the one characterizing the heat exchanger)
- No thermal energy losses to the environment
- Isentropic efficiency based on empirical performance curve
- Mass flow rate based on empirical performance curve
- Linear dependency between pump speed and volumetric flow rate

$$\dot{W} = \dot{M} \cdot \frac{\Delta p}{\eta \cdot \rho_{su}} \tag{6}$$

$$\dot{M} = \rho_{su} \cdot \varepsilon_v \cdot \dot{V}_{max} \cdot \frac{f}{50} \tag{7}$$

As stated in equation (7), the mass flow rate depends on the pump speed and on the inlet density. Since the latter (i.e. the liquid density at the given temperature) varies in a very limited range, it can be, in good approximation, considered constant throughout the simulation. This removes a non-linear equation to the system and therefore improves the model performance. In practice, the possibility is left to the user to choose between constant and variable inlet density.

Figure 8 shows the general parameters and options, and initialization values that the user has to set to use the model.

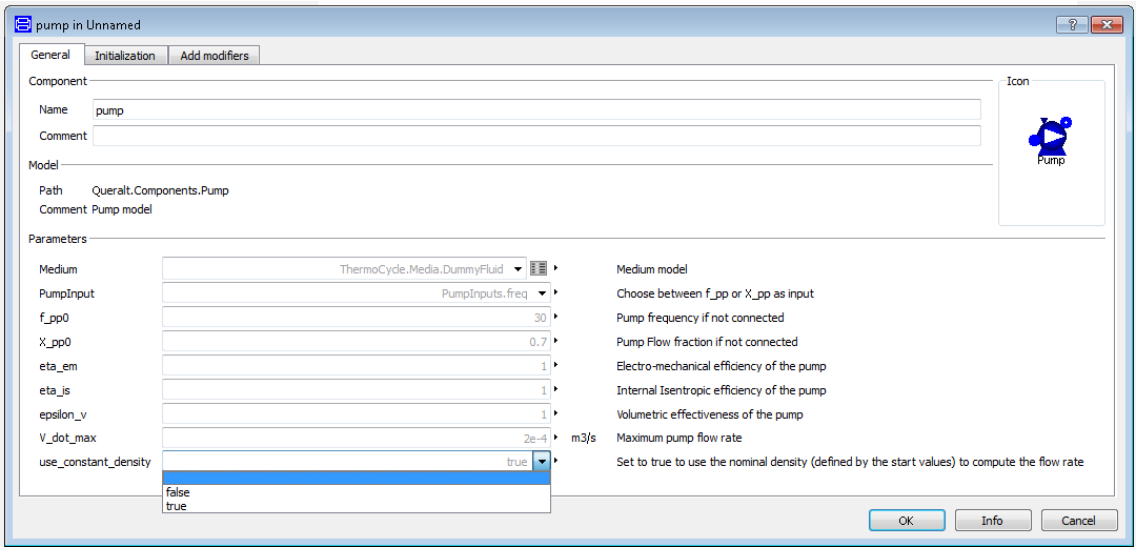

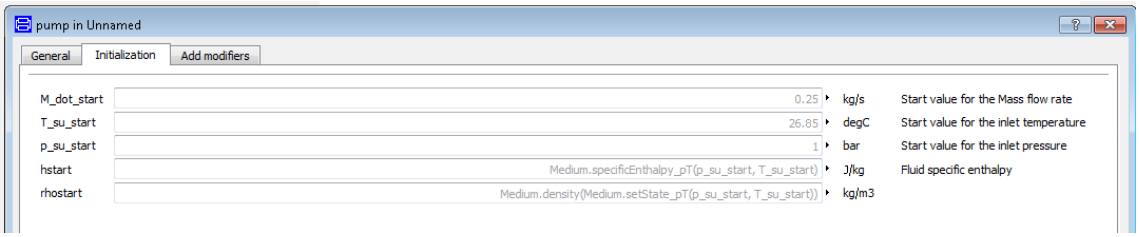

Figure 8: Parameters of the pump model

3.1.3 Heat exchanger

Model *Hx1DInc* represents the model of a counter-current plate heat exchanger in which one of the two fluids is modeled as an incompressible fluid.

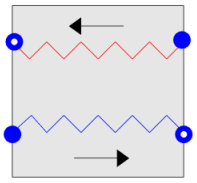

Figure 9: Icon of the heat exchanger model

It is based on the connection of different sub-components available in the ThermoCycle library (*Flow1Dim*, *Flow1dimInc*, *MetalWall*, *CountCurr*). The modeling hypotheses are the following:

- 1D Finite Volumes model (described in section 3.1.1)
- No pressure drop in the heat exchangers (they are lumped in a pressure drop component outside of the heat exchanger)
- Different heat transfer correlations are implemented
- Homogeneous flow (i.e. no slip between vapor and liquid phases)
- Neglected dynamic momentum equation

One side of the heat exchanger is modeled as a compressible flow, with the mass and energy balances being written as equations (1) and (4) in the finite volume section. This side allows computing vapor flows as well as condensation or evaporation.

The other side is considered incompressible. The mass balance equation is therefore not necessary and the energy conservation equation simplifies into equation (6).

As shown in Figure 10, different numerical options are available to increase the robustness and the computational efficiency of the model, both during initialization and during integration. Some of these options are described in section 3.1.1.

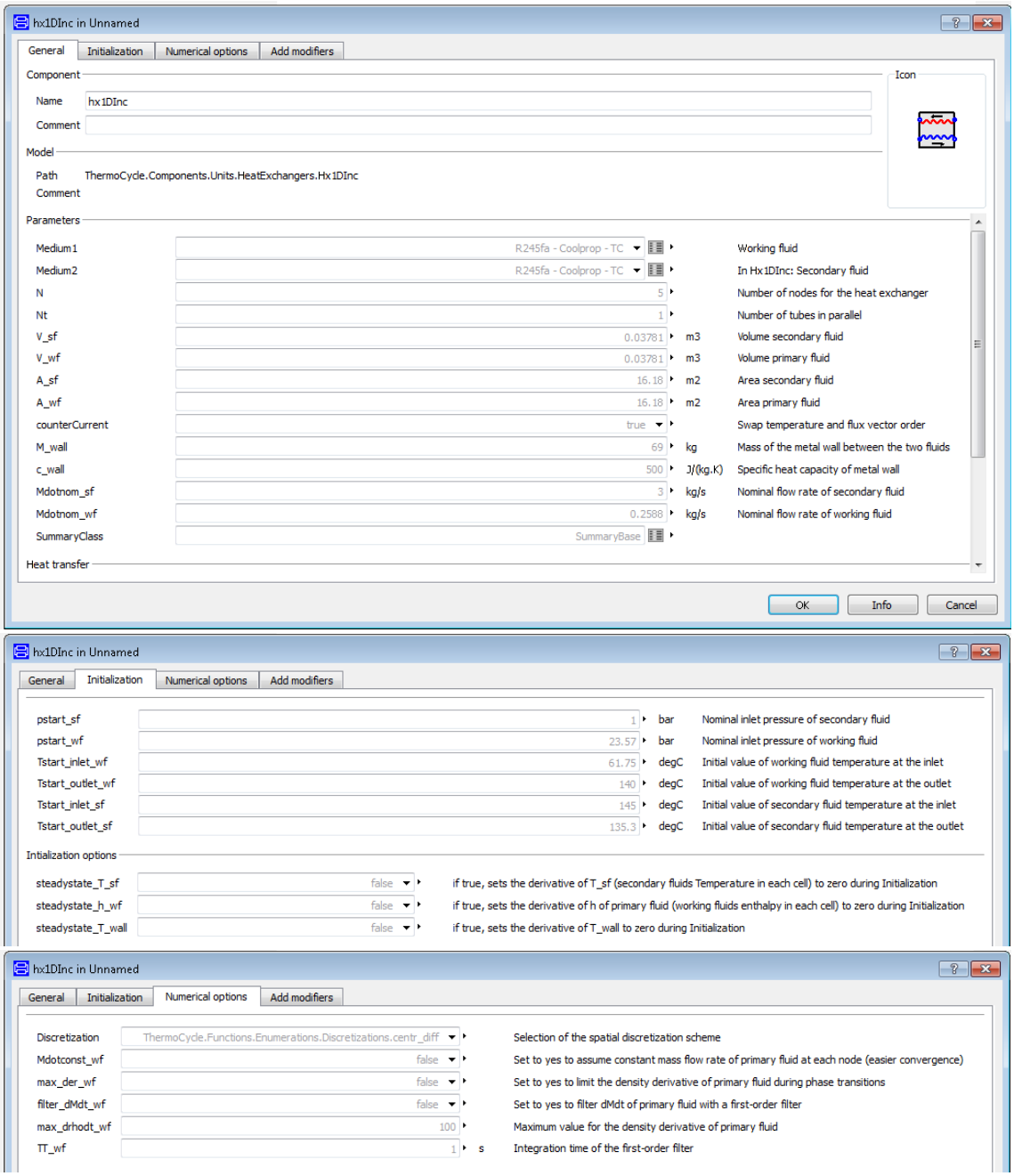

Figure 10: Parameters of the heat exchanger model

3.1.4 Pressure drop

The pressure drop (*dP*) model is a lumped model that computes a punctual pressure drop. When computing the pressure drop, the fluid is assumed incompressible, and no thermal energy losses to the enviroment are considered.

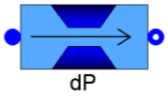

Figure 11: Icon of the pressure drop model

Three different terms are taken into account to compute the total pressure drop:

- A constant pressure difference (e.g. due to a static pressure head)
- A linear pressure drop (e.g. because of friction in a laminar flow)
- A quadratic pressure drop (e.g. turbulent flow)

Figure 12 shows some parameters and modeling options of the model. The parameter DELTAp_0 defines a limitation with which a third order polynomial expression is used instead of the quadratic expression, in order to avoid non-physical infinite derivate at this value.

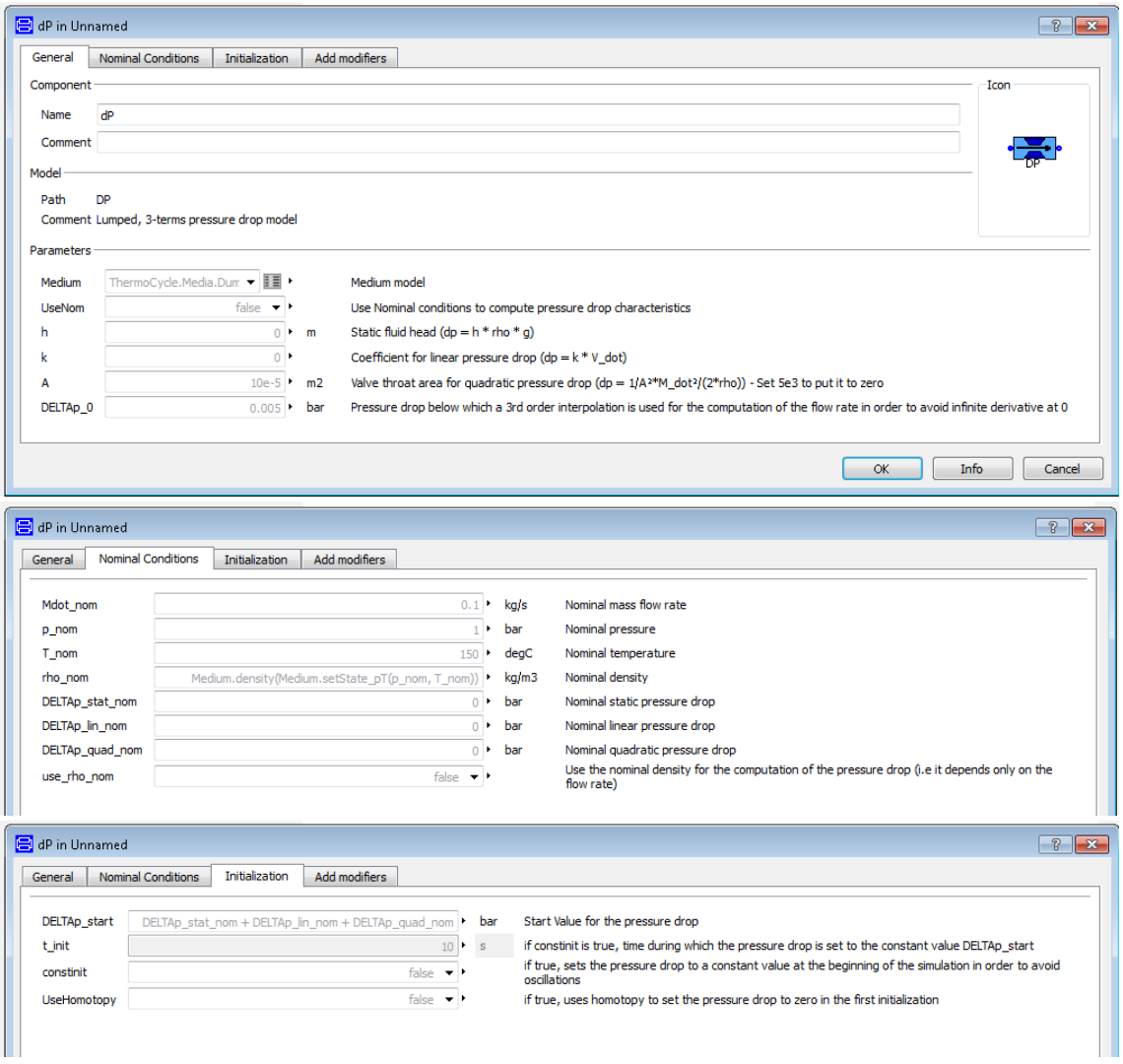

Figure 12: Parameters of the pressure drop model

3.1.5 Tank

The *Tank_pL* model was developed to simulate the effect of a liquid receiver. It is assumed to be in thermodynamic equilibrium at all times, i.e. the vapor and liquid are

saturated at the given pressure. It is modeled with a dynamic energy and mass balances and it uses L (the relative level) and p (the pressure) as state variables.

Figure 13: Icon of the *tank_pL* model

The exhaust flow rate is defined as saturated liquid while the supply flow rate coming from the inlet can be either subcooled (in which case the receiver pressure is going to decrease), saturated (in which case the receiver pressure remains constant) or two-phase (in which case the receiver pressure is going to increase).

As shown in Figure 14, the main parameter of the liquid receiver model is its internal volume. It should be noted that, the higher this volume, the easier the solving process since the tank acts as a damper and reduces the pressure fluctuations (Quoilin, 2011).

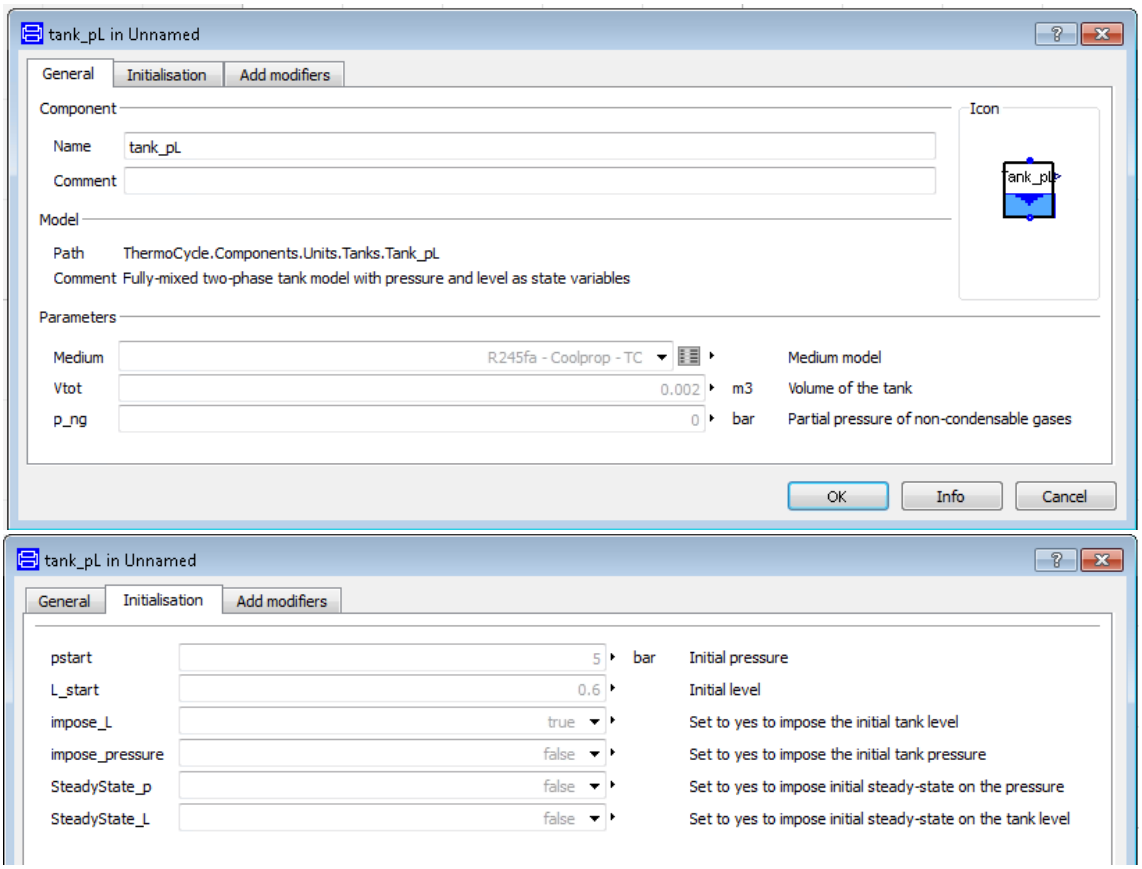

Figure 14: Parameters of the *tank_pL* model

3.1.6 Solar field

The *SolarField_Forristal_Inc* model is a solar field, composed by a loop of parabolic collectors, based on the Forristall model. (Forristall, 2003) presented a steady-state heat transfer model, which was implemented in Engineering Equation Solver (EES) and validated with monitoring data from the solar electric generating systems (SEGS) in California. This model is designed to compute the performance of a parabolic troughs solar collector's linear receiver, also called a heat collector element (HCE), and it is based on an energy balance along the collector and the HCE. The energy balance includes the direct normal solar irradiation incident on the collector, optical losses from both the collector and HCE, thermal losses from the HCE, and the heat gain into the heat transfer fluid (HTF) (Figure 15 and Figure 16).

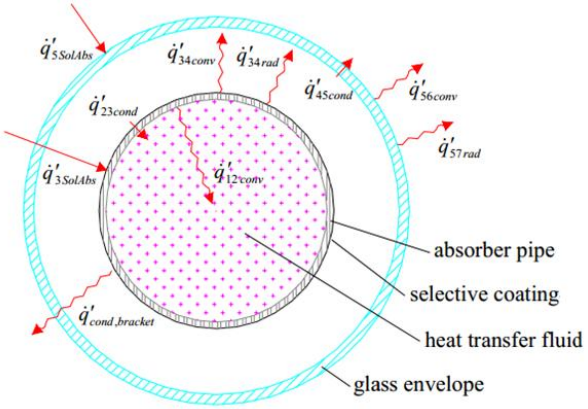

Figure 15: One-dimensional steady-state energy balance for a cross-section of an HCE (only valid for short receivers, i.e. < 100 m) (Forristall, 2003)

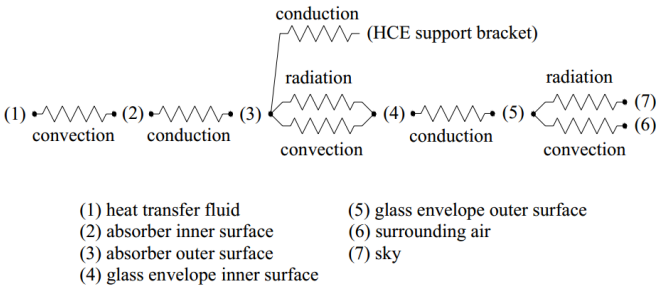

Figure 16: Thermal resistance model for a cross-section of an HCE where for clarity, the optical losses and incoming solar energy have been omitted (Forristall, 2003)

It should however be noted that Forristall model is a steady-state model, i.e. it cannot be used for rapidly fluctuating atmospheric conditions. Such a model can only be used as a quasi-steady-state model, in which with varying boundary conditions, its performance could be evaluated at every step of the solar irradiation through time, neglecting the energy accumulation in the collectors. However, this requires the dynamics in the collector to be much faster than the solar irradiation's variations in time, which does not always happen, e.g. in case of quickly-varying nebulosity.

Therefore, Forristall model has been transformed into a dynamic model that considers energy accumulation in the heat transfer fluid flow and in the metal mass. It can thus be used for transient boundary conditions. The model is available in the ThermoCycle library.

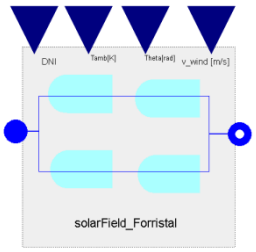

Figure 17: Icon of the solar field model

The absorber tube has been 1D-discretized because of the large ratio between diameter and length. The fluid chosen to flow through it is a synthetic thermal oil (as explained in section 4.2). The model is composed by two main sub-components, which are connected together through a thermal port:

- The *SolAbsForristal* models the dynamic one-dimensional radial energy balance around the heat collector element.
- The *Flow1DimInc* models the fluid flow as incompressible in the heat collector element (equation (5)) and the energy accumulation in the metal tube.

There are four inputs to the model representing the ambient conditions:

- DNI: Direct Normal Irradiation [W/m^2]
- Theta: Incidence angle [rad]
- T_amb: environmental temperature [K]
- v_wind: wind velocity [m/s]

As shown in Figure 18, different parameters and options are defined to use this model.

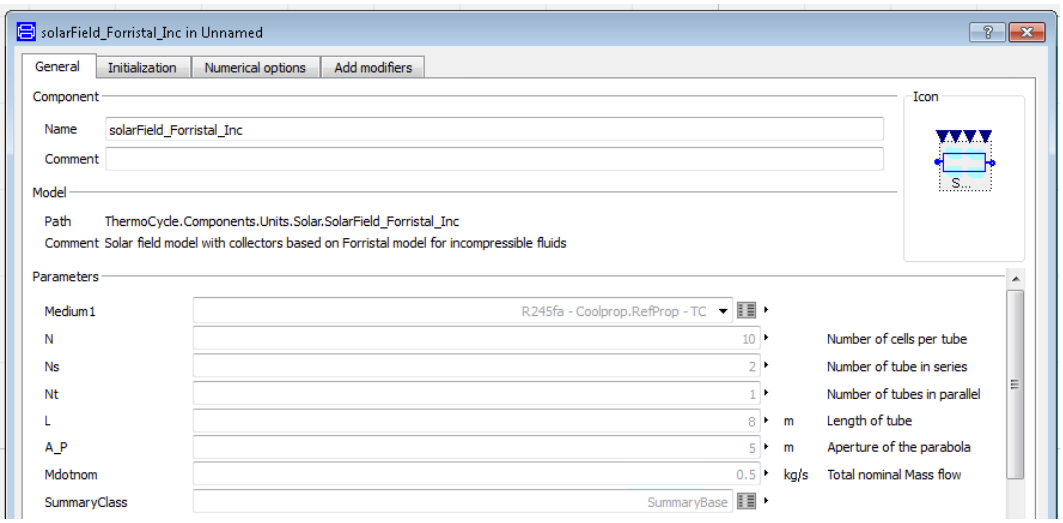

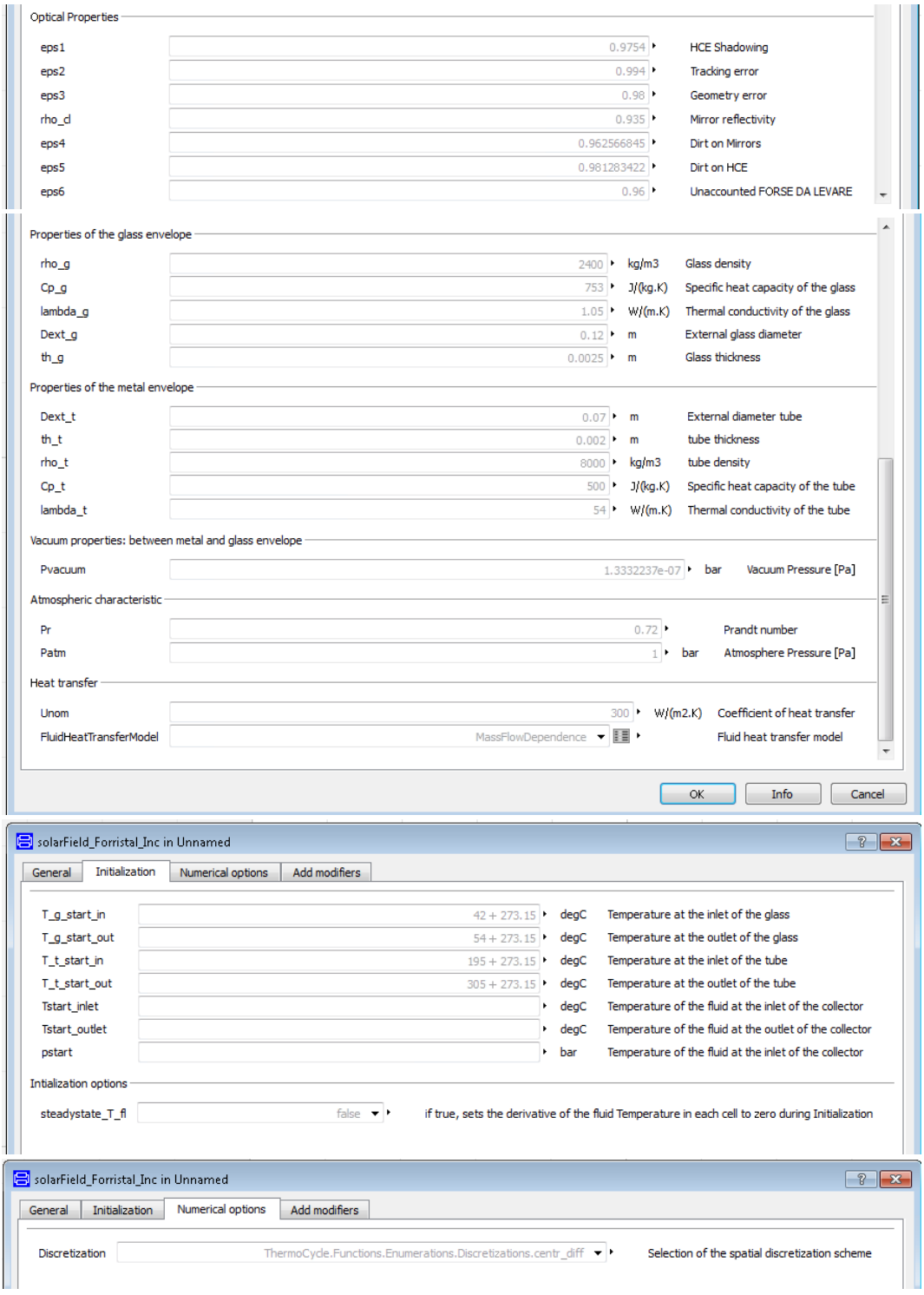

Figure 18: Parameters of the *solarField_Forristal_Inc* model

3.2 Models developed in the scope of this thesis

3.2.1 Stodola steam turbine

The model *SteamTurbine* is a steam turbine modeled by Stodola's elliptic law.

Figure 19: Icon of the turbine model

In a turbine, there is no direct relation between the rotating speed and the volumetric flow. The flow rate depends on the shape and diameter of the inlet nozzles, but also on the downward pressure. Due to the lack of information about the turbines in the CHP plant, the turbine's model has been developed using Stodola's elliptic law:

$$\dot{M} = partialArc \cdot K \cdot \sqrt{p_{su} \cdot \rho_{su}} \cdot \sqrt{1 - \left(\frac{p_{ex}}{p_{su}}\right)^2} \tag{8}$$

where K is the coefficient of Stodola's law, $\dot{M}$ is the mass flow rate, p_{su} and p_{ex} are the supply and exhaust pressures and ρ_{su} is the supply density.

The inlet mass flow rate is proportional to the *partialArc* signal if the corresponding connector is wired. In this case, it is assumed that the mass flow rate is reduced by partial arc admission, not by throttling (i.e., no loss of thermodynamic efficiency occurs) (Casella and Leva, 2009).

As stated in eq. (8), the computation of the flow rate according to Stodola depends on the turbine supply density. Computing this density requires a call to the thermodynamic properties library and can also result in an additional non-linear equation in the system. Since steam turbines usually operate with highly superheated steam, a perfect gas model can also be used, which again increases the robustness and the computational efficiency of the model. In this particular case, eq. (8) is rewritten:

$$\dot{M} = partialArc \cdot K \cdot \frac{p_{su}}{\sqrt{T_{su}}} \cdot \sqrt{1 - \left(\frac{p_{ex}}{p_{su}}\right)^2} \tag{9}$$

The choice of the real/ideal gas model is left as an option to the user.

In order to avoid numerical problems during integration, (Casella and Leva, 2009) in the ThermoPower library proposed to apply a symmetric square root approximation with finite derivative in zero. The latter term of the right-hand side becomes:

$$\sqrt{\left(1-\left(\frac{p_{ex}}{p_{su}}\right)^2\right)} \Rightarrow \frac{\left(1-\left(\frac{p_{ex}}{p_{su}}\right)^2\right)}{\sqrt{\sqrt{\left(1-\left(\frac{p_{ex}}{p_{su}}\right)^2\right)^2+0.01^2}}} \tag{10}$$

The final equation used in the model (i.e. Stodola's law in equation (8) with the approximation (10)) is plotted in Figure 20. The main advantage is that there is still a solution even if $p_{ex} > p_{su}$ (i.e. $r_p = \frac{p_{su}}{p_{ex}} < 1$), which increases the robustness of the model. If during iteration, such a situation occurs, the flow rate becomes negative, but there is no failure due to the square root of a negative number.

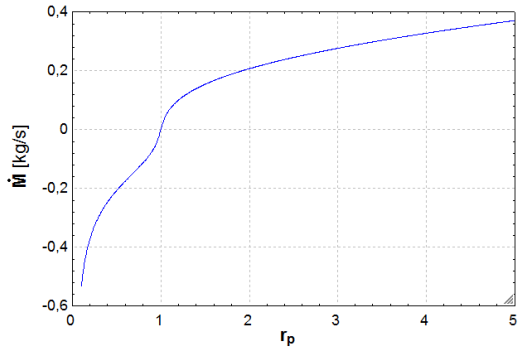

Figure 20: Mass flow rate vs. pressure ratio

It must be reminded that Stodola's law is only valid for subsonic flow conditions and multistage turbines. The main assumptions for this model are:

- Constant isentropic efficiency.
- No dynamics (it is considered negligible when compared to the one characterizing the heat exchanger).
- No thermal energy losses to the environment

Figure 21 shows the general parameters, options, initialization values and nominal conditions left to the user.

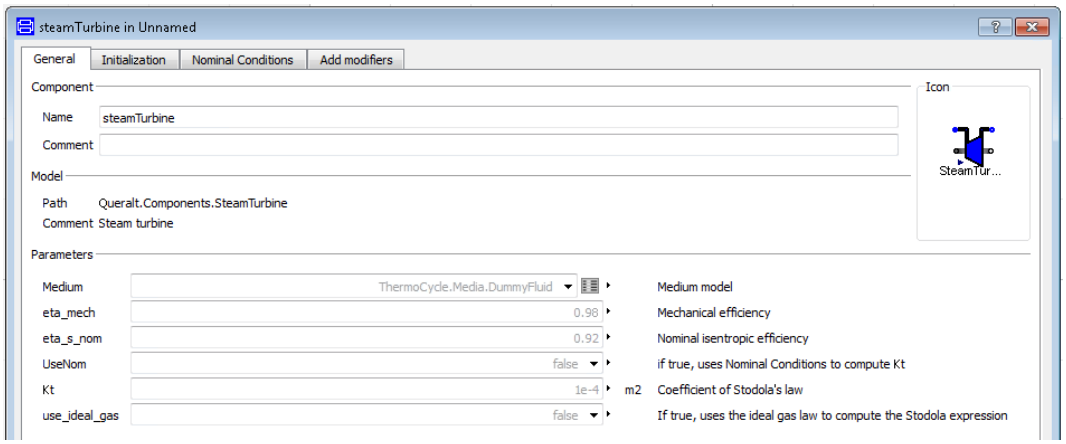

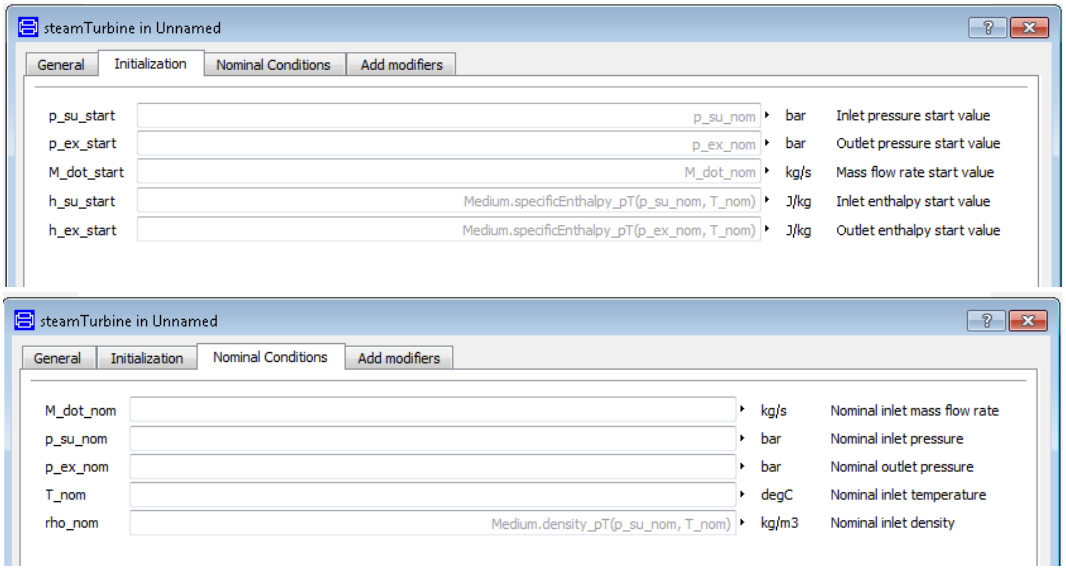

Figure 21: Parameters of the turbine model

3.2.2 Cross-flow condenser

The model *CrossCondenser* is the water-cooled condenser in the steam cycle. It is modeled as a cross-flow heat exchanger in which the working fluid is in a two-phase state and is being condensed, and the secondary fluid is in a single-phase state (i.e. liquid) and is modeled as an incompressible flow.

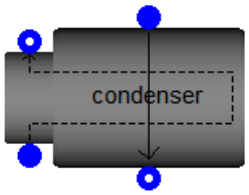

Figure 22: Icon of the *crossCondenser* model

According to the condenser datasheet (ARI, 2014), the layout is a cross-flow U-tube heat exchanger, as shown in Figure 23. The secondary fluid flows through the tubes and the working fluid flows downward from the top of the shell, remaining in liquid state at the bottom.

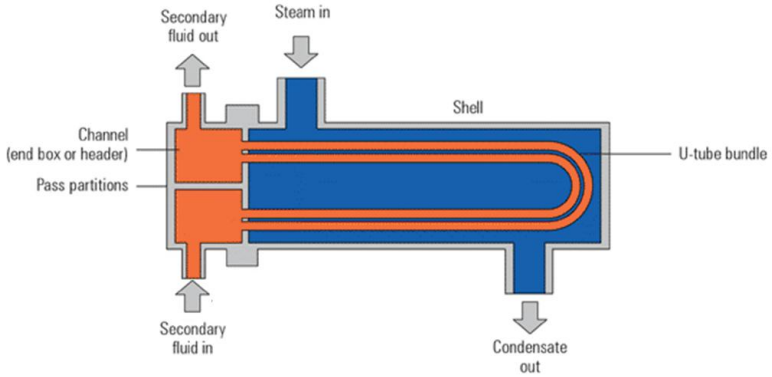

Figure 23: Internal structure of the model

In a steam condenser, the working fluid state is essentially two-phase, i.e. the subcooled liquid or superheated vapor zones being either very small or non-present. It is assumed to be in thermodynamic equilibrium at all times, i.e. the vapor and the liquid are saturated at the condenser temperature, which is considered uniform in the whole condenser. The working fluid side can therefore be modeled as a semi-isothermal heat exchanger. Its flow is thus modeled with a simple temperature source component that enables to set the saturation state. The model *SourceT* from ThermoCycle library is used for that purpose. For the working fluid, the energy balance is written:

$$\dot{M}_{wf} \cdot (h_{su} - h_{ex}) = \dot{Q}_{wf} \tag{11}$$

The condensation heat transfer coefficient is modeled by a constant thermal resistance between the metal wall and the fluid. This is achieved using the *ThermalResistance* model which is also developed and described in this chapter (see section 3.2.3).

A discretized finite volume model, subdivides the 1D cooling flow into several equal control volumes. This flow (i.e. secondary fluid in Figure 23) is a 40% propylene glycol (see Table 1) flow in a liquid state. It is therefore discretized into N incompressible cells in which the energy conservation equation is applied (eq. (5)). Due to the working fluid side is at the same saturation temperature in all the shell and since its heat transfer coefficient is assumed constant, in order to simplify the model, it is considered that the *n* U-tubes can be represented by one straight-tube with the equivalent heat exchange area and fluid volume.

The metal wall is modeled with the discretized *MetalWall* model already available in ThermoCycle. The energy balance over the wall is written:

$$c_w \cdot M_{w,i} \cdot \frac{dT_{w,i}}{dt} = \dot{Q}_{wf,i} - \dot{Q}_{sf,i} \tag{12}$$

In summary, the model is based on the connection of four different sub-components:

- *Flow1DimInc*: the flow of the secondary fluid.
- *MetalWall*: the thermal energy accumulation in the metal wall.
- *SourceT*: a heat port whose temperature is fixed at the saturation temperature of the working fluid.
- *ThermalResistance*: the thermal resistance between the metal wall and the working fluid.

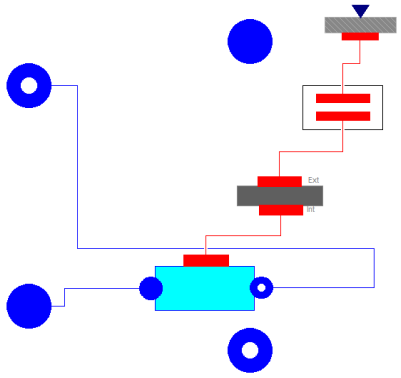

Figure 24: Diagram view of the condenser model

The heat transfer coefficient of the secondary fluid is computed using a heat transfer model available in ThermoCycle, and corresponding to a turbulent flow in a pipe. The coefficient is assumed to depend on the flow rate only, with the following relation:

$$U_{sf} = U_{nom,sf} \cdot \left(\frac{\dot{M}_{sf}}{\dot{M}_{nom,sf}} \right)^{0.8} \tag{13}$$

where U_{sf} is the computed heat transfer coefficient, $\dot{M}_{sf}$ is the actual mass flow rate, and $U_{nom,sf}$ and $\dot{M}_{nom,sf}$ are parameters of the model corresponding to the nominal values (Figure 25).

For each cell in the model, a heat exchange area, a fluid volume and a wall mass are defined:

$$A_{wf,i} = \frac{A_{wf}}{N} \; ; \; A_{sf,i} = \frac{A_{sf}}{N} \; ; \; V_{sf,i} = \frac{V_{sf}}{N} \; ; \; M_{w,i} = \frac{M_w}{N} \tag{14}$$

As shown in Figure 25, this global heat exchange area, fluid volume and wall mass are parameters of the model. The discretization scheme for the secondary fluid (described in section 3.1.1) is left to the user.

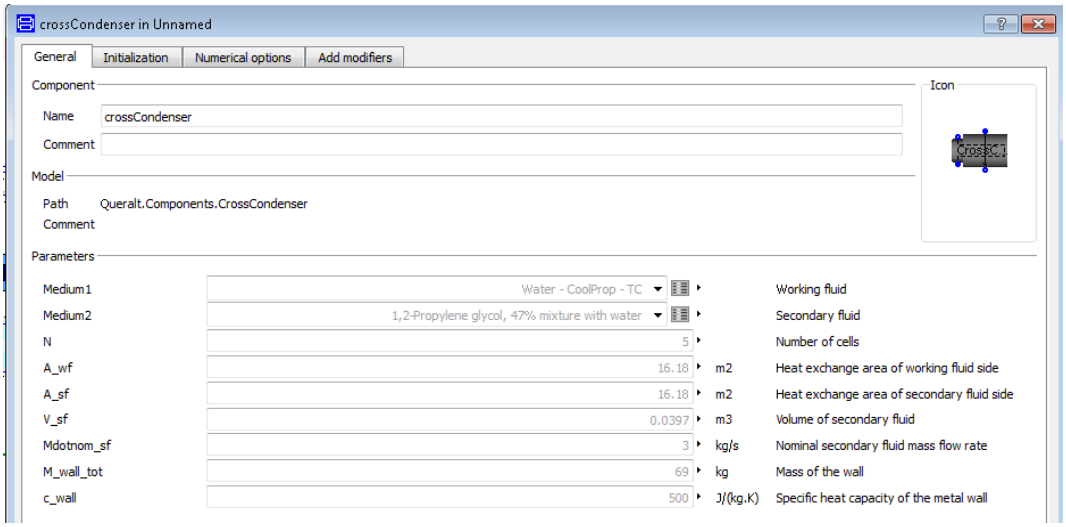

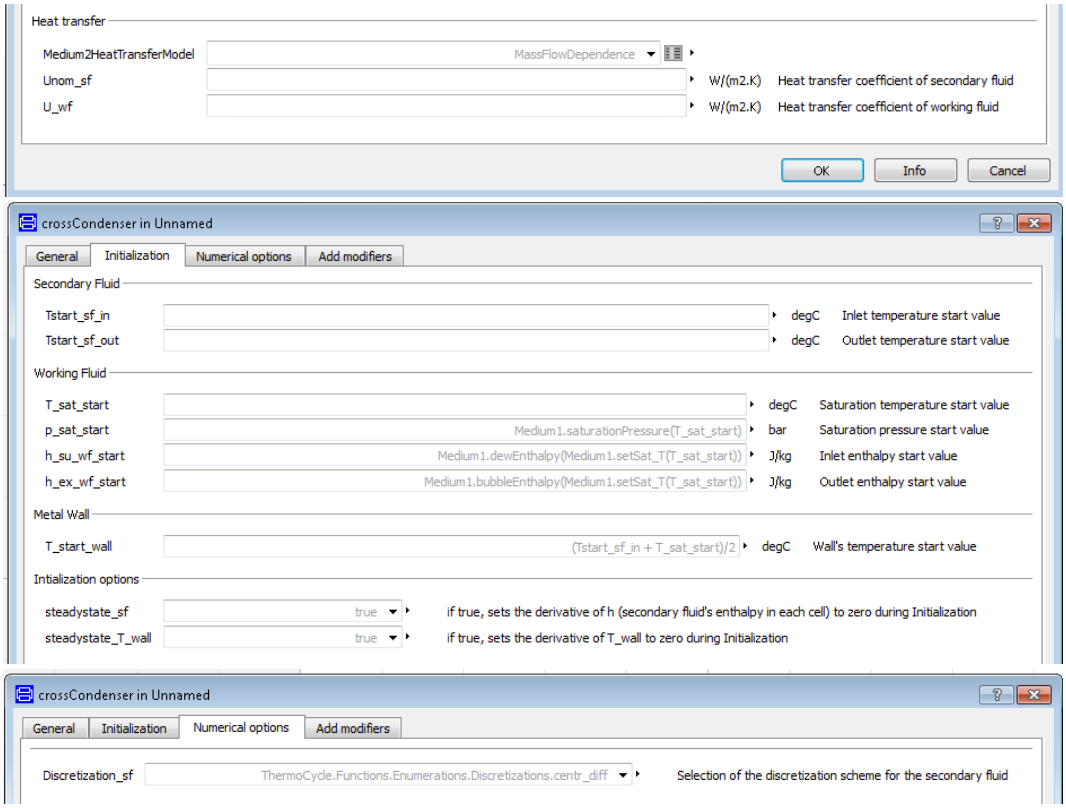

Figure 25: Parameters and options of the *CrossCondenser* model

3.2.3 Thermal resistance

Two thermal resistance models, a discretized and a non-discretized, have been developed: *ThermalResistance* and *ThermalResistanceL*.

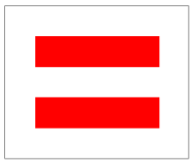

Figure 26: Icon of the thermal resistance models

These models have been created due to the need of considering the thermal resistance between the metal wall and the working fluid side in a heat exchanger, when the latter is at two-phase state and is therefore simply modeled by a thermal port at the saturation temperature (e.g. in the *crossCondenser* model).

The *ThermalResistance* model is designed for a discretized thermal resistance between two states, whose inputs are the heat exchange surface and the heat transfer coefficient (assumed constant). It is based on the use of two heat ports: the *ThermalPorts* component already available in the ThermoCycle library. These have to be connected to their respective thermodynamic states (e.g. on one hand to the working fluid source thermal port and by the other hand to the metal wall thermal

port). To define the resistance between them, both thermal ports, which are composed of *N* cells, are related by:

$$\dot{Q} = \sum \dot{Q}_i = \sum_{i=1}^{N} \left(T_{wf,i} - T_{w,i}\right) \cdot A_i \cdot U \tag{15}$$

where $A_i = \frac{A}{N}$ is the heat exchange area of each cell.

The *ThermalResistanceL* model is a non-discretized thermal resistance whose assumptions and inputs are the same as the *ThermalResistance* model but using the *ThermalPortsL* component.

As shown in Figure 27 and Figure 28, for both models the main parameters are the heat exchange area and the heat transfer coefficient, and also the number of nodes for the discretized one.

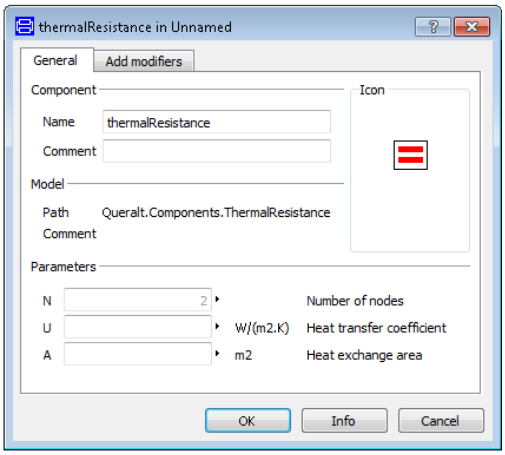

Figure 27: Parameters of the discretized thermal resistance model

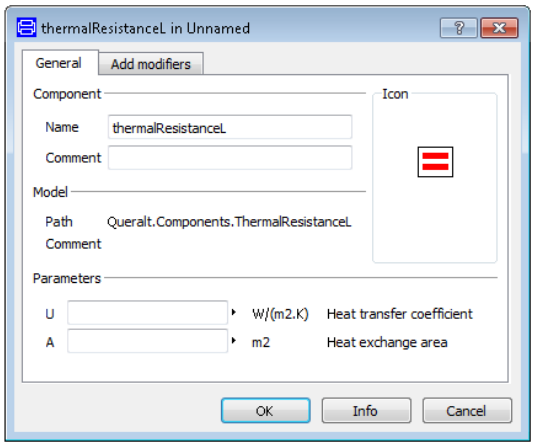

Figure 28: Parameters of the non-discretized thermal resistance model

3.2.4 Linear valve

In dynamic modeling, pressure states are usually very sensitive and can result in stiff models or in convergence failures if improper start values are provided to the Newton solver. Pressure states are generally related using pressure drop equations for turbulent flows (e.g. in case of valve). These equations are quadratic with the flow rate and therefore generate nonlinear equations. Since the present work focuses on the computational efficiency of the model, it was decided to linearize the valve equations, which dramatically simplifies the differential equation system. This hypothesis is acceptable if the modeler is not interested in the detailed simulation of the valve, which is assumed to be able to provide the required pressure drop at all times. It cannot, however, provide acceptable answers to questions such as the command of the valve, or its behavior at nearly-zero flow.

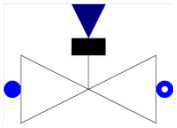

Figure 29: Icon of the valve model

Therefore, the valve pressure drop is modeled by the following linear expression using the incompressible flow hypothesis:

$$\dot{M} = cmd \cdot K \cdot \Delta p \tag{16}$$

where cmd is the valve opening and K is the fully open valve cross-sectional area ($cmd \cdot K$ is therefore the actual valve cross-sectional area).

It is assumed that the mass flow rate is proportional to the *cmd* signal if the corresponding connector is wired. If no external command is connected, it is set by the parameter X_{open} (0=fully closed; 1=fully open).

In addition to the linear hypothesis, a second simplifying option is proposed to the modeler, assuming that the valve actuates as a check-valve, i.e. no negative flow is allowed. In this case the reversal enthalpy (given by the stream connector *inFlow.h_outflow*) is set to a constant value (which will never be used). This again reduces the system of equations since the *stream* equations related to backward flows are removed.

Other assumptions for this model are:

- No dynamics (it is considered negligible when compared to the one characterizing the heat exchanger)
- No ambient heat losses (the expansion is assumed isenthalpic)

As shown in Figure 30, there is an option left to the user that allows computing the cross-sectional area of the fully open valve using the nominal conditions, instead of setting its value as a parameter.

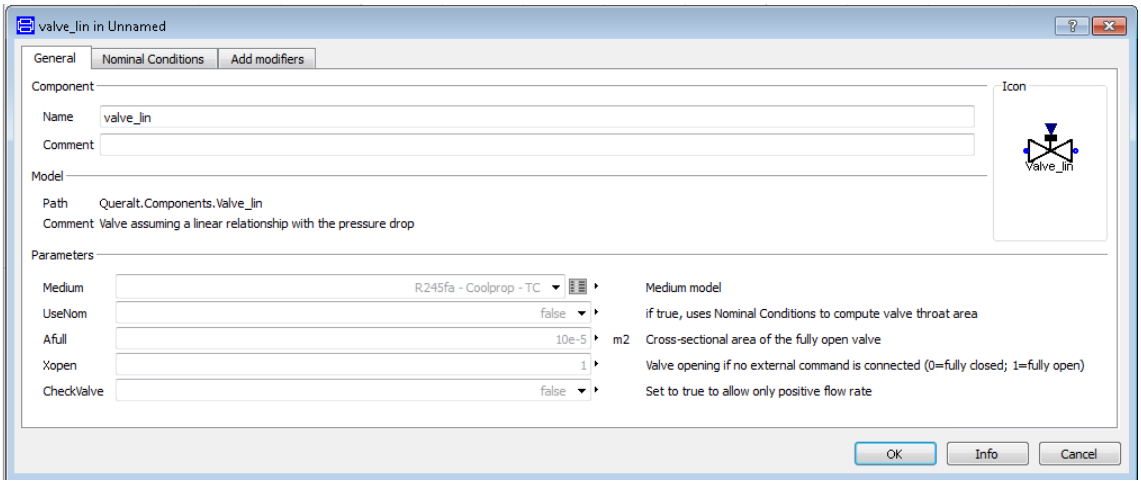

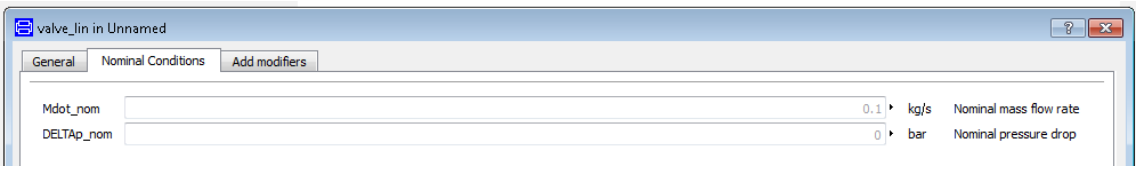

Figure 30: Parameters of the linear valve model

3.2.5 Two-phase drum

The *Drum_pL* model is a two-phase drum model with pressure and relative level as state variables. This model has one inlet and two outlets (one for vapor and the other for liquid). It is assumed to be in thermodynamic equilibrium at all times inside the control volume, i.e. the vapor and liquid are saturated at the drum pressure.

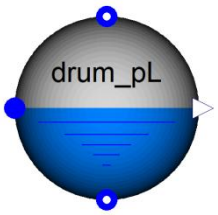

Figure 31: Icon of the *drum_pL* model

Usually, two-phase tanks are modeled by the energy and mass conservation laws, using pressure and enthalpy as state variables (some examples can be found in ThermoPower or ThermoSyspro libraries) as shows the following equation:

$$\frac{dH}{dt} = \sum \dot{M}_{su} \cdot h_{su} - \sum \dot{M}_{ex,l} \cdot h_l - \sum \dot{M}_{ex,v} \cdot h_v + V \cdot \frac{dp}{dt} \qquad (17)$$

However it should be noted that, focusing on the start values, enthalpy is not entirely convenient as a state variable because its initial value can be difficult to set. In additional a call to the thermophysical properties libraries in two-phase state with (p,h) as inputs requires both a “traditional” call and a call to the saturation properties with p as input. Since most EOS are explicit in temperature and density these calls require iterations and are time-consuming. Their number should therefore be limited to minimum value in any dynamic model.

Therefore, a model with pressure (p) and relative liquid level (L) as state variables is developed. This approach solves the issue of the start values (pressure and level are very accessible values to set) and only requires one saturation call to the thermodynamic properties.

The mass conservation law for the fixed two-phase liquid/vapor control volume is written (Lu, 1999):

$$\frac{dM}{dt} = \frac{d(\rho_l \cdot V_l + \rho_v \cdot V_v)}{dt} = \dot{M}_{su} - \dot{M}_{ex,l} - \dot{M}_{ex,v} \qquad (18)$$

where V_l and V_v are the volumes of liquid and vapor, ρ_l and ρ_v are their saturation densities and $\dot{M}_{su}$, $\dot{M}_{ex,l}$ and $\dot{M}_{ex,v}$ are the supply and exhaust mass flow rates. For a constant volume $V = V_l + V_v$ and considering the relative liquid level $L = V_l/V$, the left-hand side term expanded into pressure and level derivatives is therefore expressed as:

$$\begin{aligned}\frac{d(\rho_l \cdot V_l + \rho_v \cdot V_v)}{dt} &= V \cdot \frac{d(\rho_l \cdot L + \rho_v \cdot (1-L))}{dt} \\ &= V \cdot \left[(\rho_l - \rho_v) \cdot \frac{dL}{dt} + \left(L \cdot \frac{d\rho_l}{dp} + (1-L) \cdot \frac{d\rho_v}{dp}\right) \cdot \frac{dp}{dt}\right]\end{aligned} \tag{19}$$

The mass balance is finally written:

$$V \cdot \left[(\rho_l - \rho_v) \cdot \frac{dL}{dt} + \left(L \cdot \frac{d\rho_l}{dp} + (1-L) \cdot \frac{d\rho_v}{dp}\right) \cdot \frac{dp}{dt}\right] = \dot{M}_{su} - \dot{M}_{ex,l} - \dot{M}_{ex,v} \tag{20}$$

The energy balance for the fixed two-phase liquid/vapor control volume is written:

$$\frac{dU}{dt} = \frac{d(\rho_l \cdot V_l \cdot u_l + \rho_v \cdot V_v \cdot u_v)}{dt} = \dot{M}_{su} \cdot h_{su} - \dot{M}_{ex,l} \cdot h_l - \dot{M}_{ex,v} \cdot h_v + \dot{Q} + \dot{W} \tag{21}$$

where V_l and V_v are the volumes of liquid and vapor, ρ_l and ρ_v are their saturation densities, u_l and u_v are their internal energies, $\dot{M}_{su}$, $\dot{M}_{ex,l}$ and $\dot{M}_{ex,v}$ are the supply and exhaust mass flow rates, h_{su} , h_l and h_v are the supply enthalpy and the exhaust saturation enthalpies, $\dot{Q}$ is the heat supply and $\dot{W}$ is the internal work. The latter is null for a constant volume $V = V_l + V_v$. Considering the relative liquid level $L = V_l/V$ and recognizing that $u_i = h_i - {}^{p}/_{\rho_i}$, the left-hand side term expanded into pressure and level derivatives is therefore expressed as:

$$\begin{aligned}\frac{d(\rho_l \cdot V_l \cdot u_l + \rho_v \cdot V_v \cdot u_v)}{dt} &= V \cdot \frac{d(\rho_l \cdot L \cdot h_l + \rho_v \cdot (1-L) \cdot h_v - p)}{dt} \\ &= V \\ &\cdot \left[(\rho_l \cdot h_l - \rho_v \cdot h_v) \cdot \frac{dL}{dt}\right. \\ &\left. + \left[L \cdot \left(\rho_l \cdot \frac{dh_l}{dp} + h_l \cdot \frac{d\rho_l}{dp}\right) + (1-L) \cdot \left(\rho_v \cdot \frac{dh_v}{dp} + h_v \cdot \frac{d\rho_v}{dp}\right) - 1\right] \cdot \frac{dp}{dt}\right]\end{aligned} \tag{22}$$

The energy balance is finally written:

$$\begin{aligned}V \cdot \left[(\rho_l \cdot h_l - \rho_v \cdot h_v) \cdot \frac{dL}{dt} + \left[L \cdot \left(\rho_l \cdot \frac{dh_l}{dp} + h_l \cdot \frac{d\rho_l}{dp}\right) + (1-L) \cdot \left(\rho_v \cdot \frac{dh_v}{dp} + h_v \cdot \frac{d\rho_v}{dp}\right)\right] \cdot \frac{dp}{dt}\right] \\ = \dot{M}_{su} \cdot h_{su} - \dot{M}_{ex,l} \cdot h_l - \dot{M}_{ex,v} \cdot h_v + \dot{Q} + V \cdot \frac{dp}{dt}\end{aligned} \tag{23}$$

In both the mass (20) and energy (23) conservation equations, the variables are either extrinsic variables or are saturation variables directly computed from the value of p.

These equations are therefore entirely defined by the two variables p and L which can be selected as state variables by the solver.

As shown in Figure 32, p and L are the initialization values. As for the *tank_pL* model (section 3.1.5), the volume of the drum is the main parameter. Generally speaking, the higher this volume, the easier the solving process since the tank acts as a damper and reduces the pressure fluctuations (Quoilin, 2011).

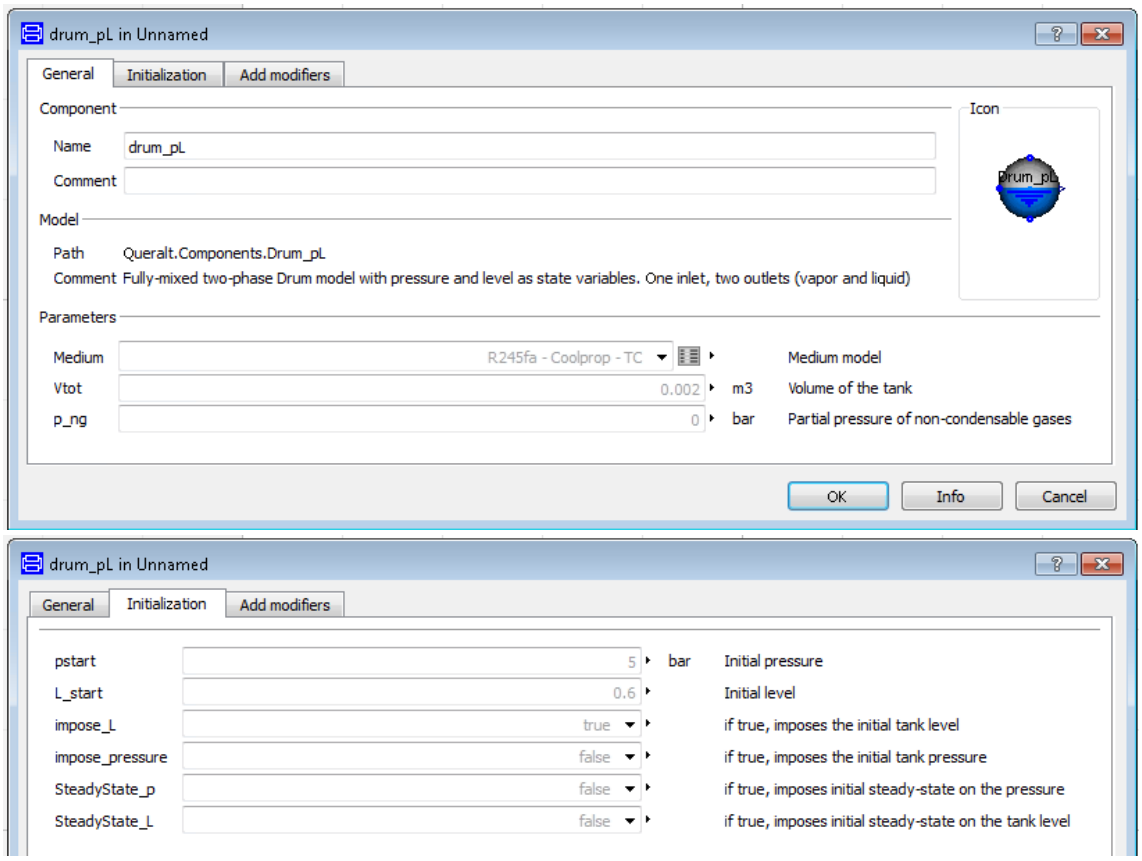

Figure 32: Parameters of the *Drum_pL* model

For the purpose of building an overall cycle model, two models based on the *Drum_pL* model have been developed, in which the model equations remain the same but the number of inlets has been increased to represent visual, realistic components: the drum of the boiler system and a deaerator.

Boiler Drum

The Boiler Drum model is a variation of the *Drum_pL* model in which there are two inlet flanges instead of one: one for the feed water flow coming from the economizer and another for the flow coming from the evaporator, to represent the drum in the boiler system. There are two outlets: a liquid one for the flow going out to the evaporator and a vapor one for the saturated steam mainly going to the superheater section but also going to the deaerator.

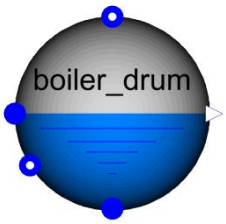

Figure 33: Icon of the *Boiler_drum* model

The parameters and modeling options for this model are the same that for the *Drum_pL* model, already shown in Figure 32.

Deaerator

The *Deaerator* model is a variation of the *Drum_pL* model in which there are two inlet ports instead of one, corresponding to a tray-type deaerator. This type of deaerator can be modeled as liquid vapor tank in which saturated vapor is injected to extract the air dissolved in the liquid. An extraction port allows removing the air/steam mixture. In the present model, the infiltration of non condensing gases is not modeled. The working fluid is always considered as pure water. The extraction port is therefore not used, but the injection of superheated vapor is modeled to remain as close to reality as possible.

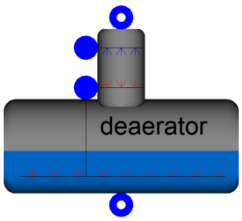

Figure 34: Icon of the *deaerator* model

The upper inlet port represents the boiler feed water, which enters the vertical domed deaeration section above the perforation trays and flows downward through them, ending into the horizontal storage vessel from where it will be pumped to the boiler system.

The lower inlet port represents the low-pressure heated steam, which firstly enters below the perforation trays and flows upward through them, stripping the dissolved gas from the boiler feed water and exiting at the top of the domed section via the vent. And secondly, it also enters into the horizontal storage vessel through a sparge pipe in order to keep the stored deaerated water warm.

The parameters and modeling options for this model are the same that for the *Drum_pL* model, already shown in Figure 32.

3.2.6 Heat exchangers

As stated above, to ensure the robustness as well as the computational efficiency of the simulation and due to the lack of information about the heat exchangers geometry inside the boiler system (e.g., economizers, evaporator and superheaters), a simplified heat exchanger model based on the ε-NTU or LMTD methods has been developed. These methods were created for steady-state simulation and are not suitable for dynamic modeling because transient conditions, which usually involve the crossing of the temperature profiles (negative pinch point), would lead to numerical errors. However, in this work, these methods have been modified to be readily usable, even in dynamic models.

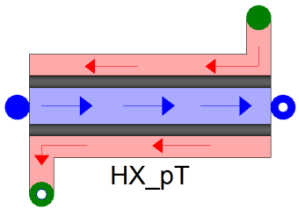

Figure 35: Icon of the heat exchanger model

The proposed model is not discretized, and therefore does not make use of the traditional finite volume approach, which as previously mentioned involves many thermodynamic property calls and multiplies the number of nonlinear equations. Therefore, two different heat exchangers are developed for both single- (i.e., economizer, super-heaters) and two-phase (i.e., evaporator) state of the working fluid.

The secondary fluid is a heat transfer fluid, which can for example be the flue gases at the exhaust of the furnace during the biomass combustion, or the thermal oil coming from a field of parabolic troughs. Usually, the properties of incompressible fluids such as these ones are defined with polynomials or tables explicit in temperature. Hence, if enthalpy is used as an input, the solver has to numerically compute its value, which requires iterations on the temperature to find the desired enthalpy. Therefore, the connectors used for the secondary fluid use pressure and temperature as state variables. The main advantages are explained in section 3.2.9.

Finally, it is important to note that the proposed heat exchanger models account for energy accumulation, but not for mass accumulation: the outlet flow rate is always exactly equal to the inlet flow rate. This is an important hypothesis that will have to be validated. As a result, in a steam plant, mass accumulation only occurs in the drum or tank components (see sections 3.1.5 and 3.2.5).

Single phase heat exchanger

The *HX_singlephase_pT* model is a non-discretized counter-current heat exchanger where both working and secondary fluids are single-phase and are modeled by means of the LMTD method.

This model is intended to be very simple, in order to maximize the robustness and the rapidity of the simulation, but maintaining its validity. It is a non-discretized model in which some dynamics have been included in the form of a thermal mass. Contrary to a steady-state model, the heat transfer problem is divided in two:

- A first heat transfer between the hot fluid and the wall
- A second heat transfer between the wall and the cold fluid

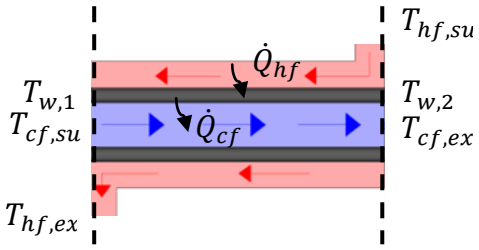

Figure 36: Sketch of the variables used in the model

The metal wall is considered as a thin wall (i.e., no temperature gradient through the wall thickness). The two computed heat flows are not necessarily equal, the difference between them corresponding to the heat accumulation or rejection of the metal wall (see Figure 36), which is accounted for by the following equation:

$$M_w \cdot c_w \cdot \frac{dT_w}{dt} = \dot{Q}_{hf} - \dot{Q}_{cf} \tag{24}$$

where M_w is the mass of the wall, c_w is the specific heat capacity of the metal wall, T_w is the mean temperature in the wall, and $\dot{Q}_{hf}$ and $\dot{Q}_{cf}$ are the heat power transferred by the hot fluid and received by the cold fluid. The above equation allows computing the average wall temperature, but not the temperature gradient within the wall. A modeling assumption is therefore needed: the temperature gradient through the wall length is considered linear and is the average of the temperature gradient in each fluid weighted by their respective thermal conductances:

$$T_{w,2} - T_{w,1} = \frac{AU_{cf} \cdot \left(T_{cf,ex} - T_{cf,su}\right) + AU_{hf} \cdot \left(T_{hf,su} - T_{hf,ex}\right)}{AU_{cf} + AU_{hf}} \tag{25}$$

Figure 37 shows all the parameters and modeling options of the model. The *Use_AU* option allows the user to use a global thermal conductance (i.e. the global heat transfer coefficient is calculated by considering two convective heat transfer resistances in series, assuming constant area) instead of setting two different heat exchange areas.

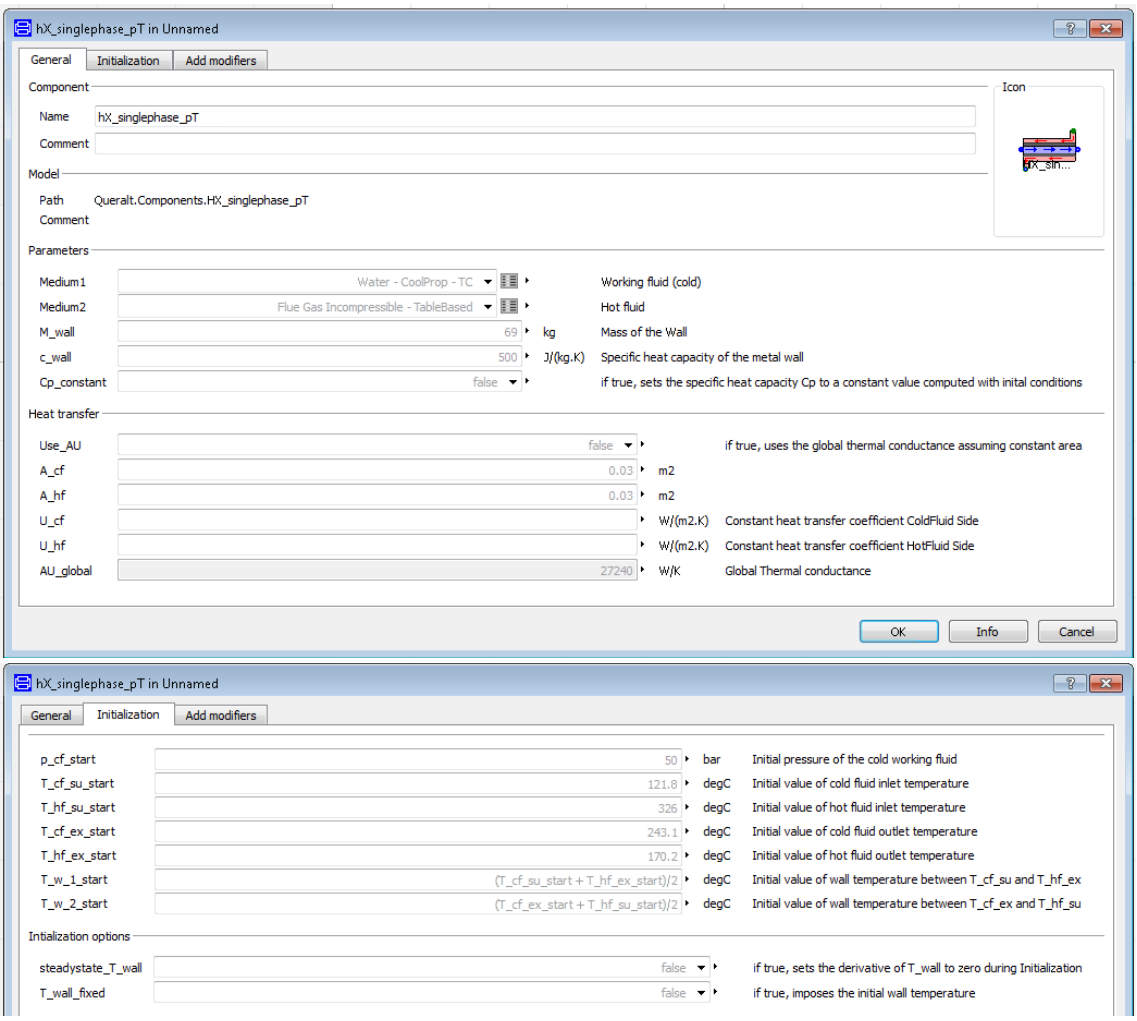

Figure 37: Parameters for the single-phase heat exchanger model

Method LMTD: function *LMTD_robust*

The heat exchanger model comprises three different temperature profiles: the secondary fluid, the wall and the working fluid. As previously mentioned, the goal is to compute the two heat flows using the LMTD method, which is applied twice: between the secondary fluid and the wall, and between the wall and the working fluid temperature profiles.

However, in dynamic simulation some profiles can cross each other for a small period of time, which impedes the use of this method. Furthermore during the initialization process, temperature profiles are highly variable, which can also lead to simulation failures if they cross in any moment.

In (Quoilin, 2011), a formalism was set up to avoid numerical failures during the iterations of the Newton solver (i.e. for steady-state simulation only). The idea behind this method is to rewrite the heat transfer model using casual equations only, instead of leaving the iterative process to the solver. This method presents the advantage of

allowing conditional statement and therefore brings a solution if negative pinch points appear during the iterations, by modifying the LMTD equation to avoid logarithms of negative numbers.

The method proposed by (Quoilin, 2011) has been reformulated for dynamic simulation and extended to ensure the smoothness of the method. This has been done in the *LMTD_robust* function, whose code is provided below:

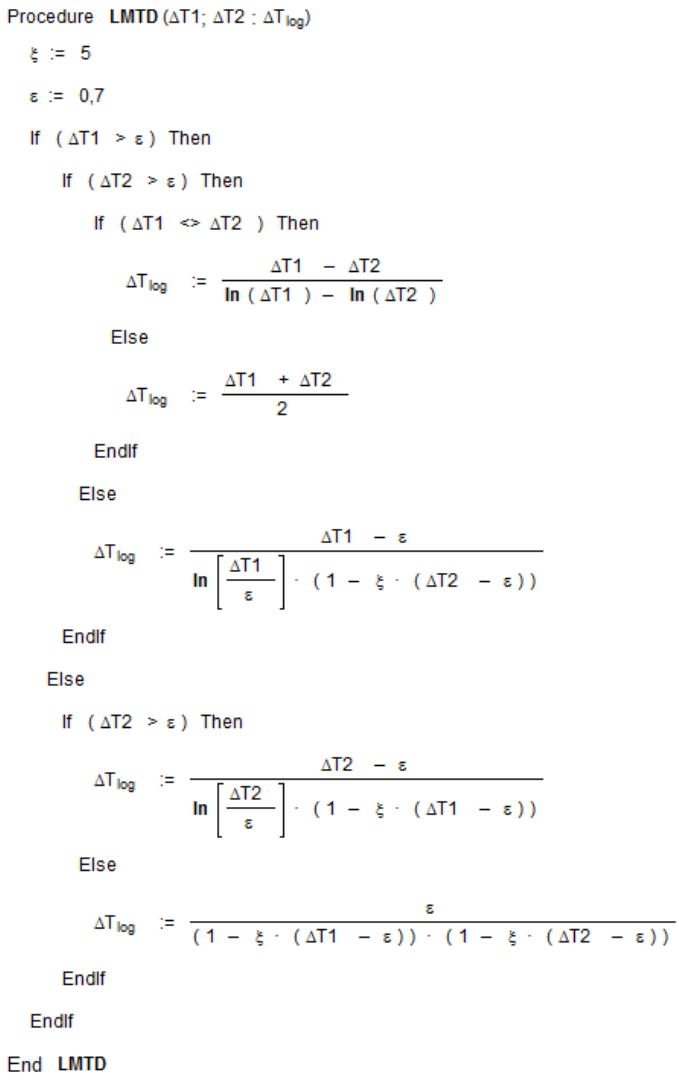

Figure 38: Code of the *LMTD_robust* function

where ε and ξ are two parameters to set by the user whose role will be explained below.

An isometric view of a 3-D representation of the *LMTD_robust* function for a range of temperature gradients between the working or secondary fluid and the wall is shown in Figure 39. Temperature differences on the two sides of the heat exchanger vary from minus one to three Kelvin. The position of the grids corresponds to DELTAT=0.

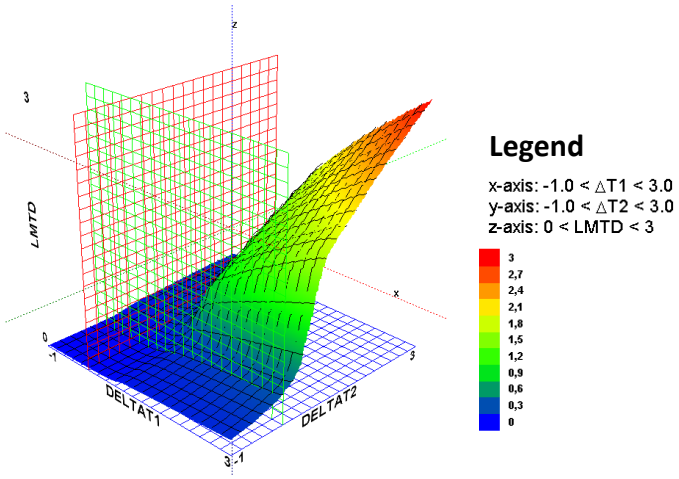

Figure 39: 3-D plot of the *LMTD_robust* function

An important highlight of function *LMTD_robust* is that it is C0-continuous, which is important for the solver in order to avoid problems, e.g. those caused by infeasible systems of equations. Nonetheless, it can be seen in Figure 40 that the derivatives of the function are not continuous. A modification of the *LMTD_robust* function with splines functions could be implemented to make it C1-continuous, which would increase the computational efficiency of the heat exchanger model.

As shown in Figure 39, LMTD depends on the two temperature differences. It should moreover be noticed that *LMTD_robust* is non-null when ΔT = 0, what means that there is always a leakage heat flow (although it can be neglected).

In this manner, the function is computable even for negative temperature gradients. This allows the solver to continue with the simulation instead of causing a failure, e.g. at some point when the temperatures profiles could cross. However, it must be noticed that a positive LMTD value when pinch points are negative lead to a non-physical behavior: it leads to a positive heat flow for a negative temperature differences, i.e. the heat flow is being transferred from the cold to the hot side.

Therefore, LMTD value for negative pinches should be as small as possible so that the leakage heat flow can be neglected. Parameters ε and ξ play a key role at this point:

- $\boldsymbol{\xi}$ represents the rapidity in which LMTD goes to zero. The latter increases with ξ, as it can be seen in Figure 40. Small ξvalues lead to higher LMTD values which, as previously mentioned, is not physically correct. However, too high ξvalues entail steep variations of the *LMTD_robust* function, which can also lead to simulation failures.

- $\boldsymbol{\varepsilon}$ is the threshold (in terms of DELTAT value) below which the LMTD function is replaced by a decreasing polynomial function (see Figure 38). It should therefore be set to a lower value than the “natural” pinch points of the modeled heat

exchangers in order to ensure the validity of the LMTD method in "usual" operating conditions (e.g., in Figure 40 the purple result would be only valid if the threshold is lower than ΔT_2 = 2K). As for ξ, it should however not be too small to avoid slow and non-robust simulation.

Figure 40 is a comparative plot of the *LMTD_robust* when changing the parameters ε and ξ, for the range of temperature gradient $\Delta T_2 \in (-1\,,3)$ and if ΔT_1 is at the constant value of 2 K. The original LMTD method has also been plotted.

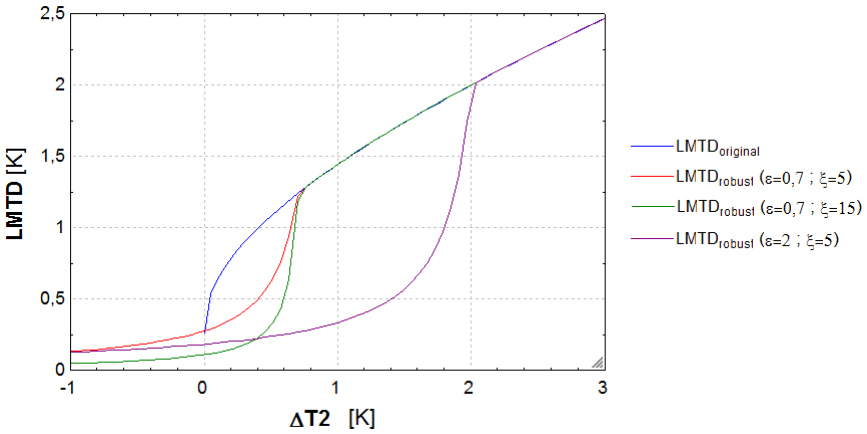

Figure 40: Plot of three different LMTD robust function and original LMTD function

Figure 41, Figure 42 and Figure 43 present three 3-D surface of the *LMTD_robust* function, with different values for the parameters. LMTD original function has also been plotted in Figure 44.

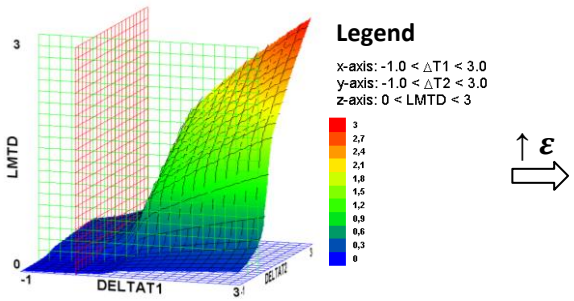

Figure 41: $\varepsilon = 0.7\ ;\ \xi = 5$

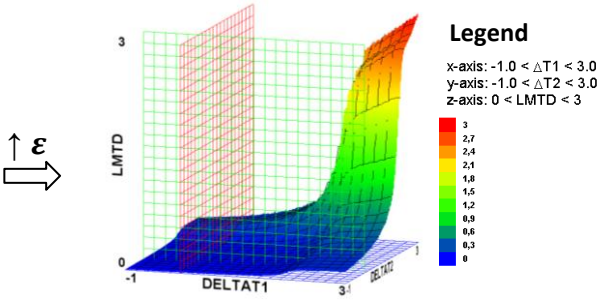

Figure 42: $\varepsilon = 2\ ;\ \xi = 5$

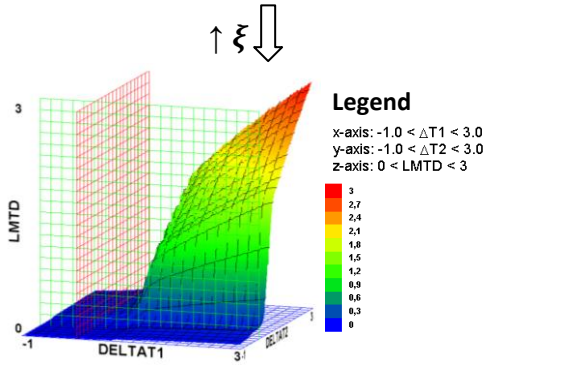

Figure 43: $\varepsilon = 0.7\ ;\ \xi = 15$

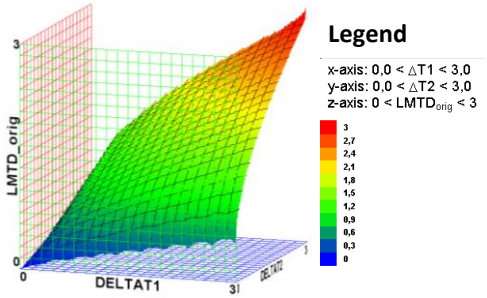

Figure 44: LMTD original

Two-phase heat exchanger

The *HX_twophase_pT* model is a non-discretized counter-current heat exchanger model in which the working fluid (cold) is in a two-phase state and the secondary fluid (hot) is modeled based on the ε-NTU method for semi-isothermal heat exchangers.

The working fluid is assumed to be in thermodynamic equilibrium at all times, i.e. the steam and water are saturated at the evaporation pressure and temperature. Its flow is thus modeled with a simple temperature source component that enables to set the saturation state. The model *SourceT* from ThermoCycle library is used for that purpose. For the working fluid (isothermal), the energy balance is written:

$$\dot{M}_{iso} \cdot (h_{ex} - h_{su}) = \dot{Q}_{iso} \tag{26}$$

The two-phase heat exchange is modeled in a very similar manner as the single phase heat exchanger. There are three temperature profiles (the wall temperature profile is in the middle) and two heat flows are computed (between the hot fluid and the wall and between the wall and the cold evaporating fluid).

However, contrary to the previous model, it is assumed that the wall temperature is uniform throughout the heat exchanger. This hypothesis can be justified by the fact that heat transfer coefficients are usually much higher on the evaporating fluid side (i.e. the isothermal side) than on the secondary fluid side. The heat transfer between the wall and the cold fluid (both isothermal) is therefore given by:

$$\dot{Q} = AU_{iso} \cdot (T_w - T_{iso}) \tag{27}$$

Another difference with the single-phase model is that the heat flow of the secondary (hot) fluid is computed with the ε-NTU method instead of the LMTD method. This is achieved by using the *Semi_isothermal_HeatExchanger_pT* model (see below).

Figure 45 shows the main parameters and options of the model.

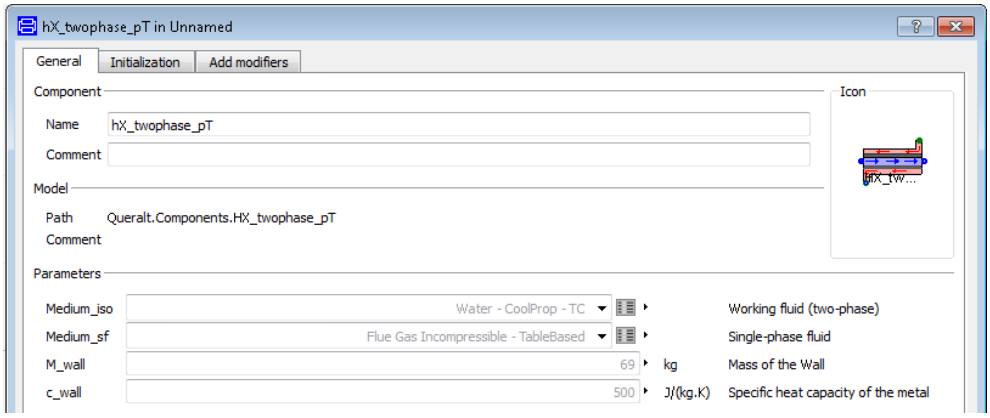

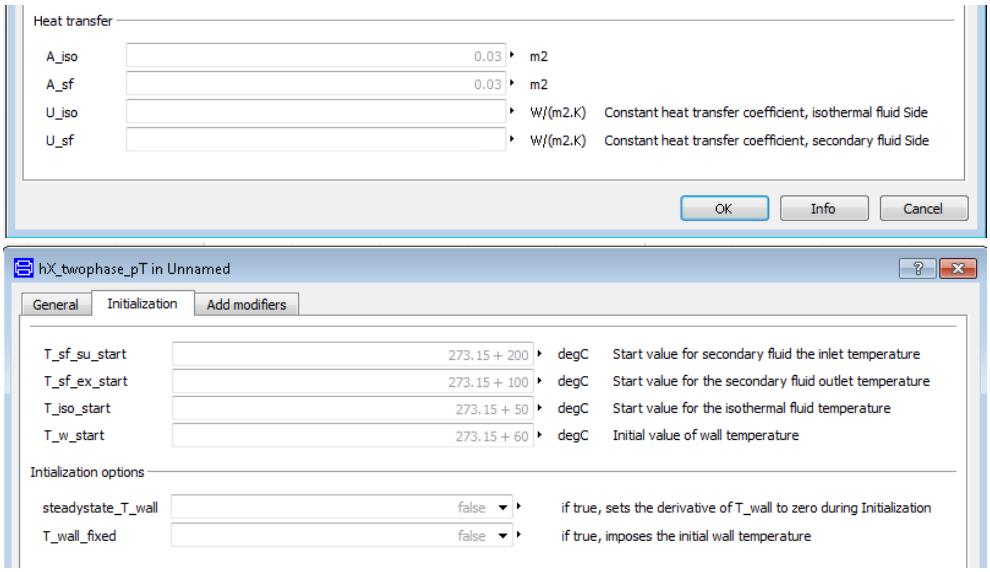

Figure 45: Parameters and options of the two-phase heat exchanger

Semi isothermal heat exchanger

This model is based on the *Semi_isothermal_HeatExchanger* model already available in ThermoCycle, with some minor modifications. The connectors have been changed from (p,h) to (p,T) connectors (see section 3.2.9).

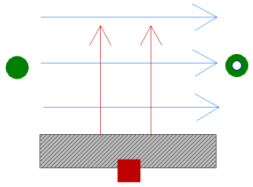

Figure 46: Icon of the *Semi_Isothermal_HeatExchanger_pT* model

Using these connectors, some equations can be simplified. For example, there is no need to define two states to compute the supply and exhaust temperatures since they are already the state variables transmitted through the connectors. The energy conservation equation is written:

$$\dot{Q} = \dot{C} \cdot (T_{su} - T_{ex}) \tag{28}$$

Because this component allows flow reversal, its heat transfer is computed by means of the specific heat capacity of the mean state (i.e., the temperature is an average between the inlet and outlet ones). Two different temperature profiles are considered (i.e. one for the fluid, one for the isothermal wall). The heat transfer between these profiles is written:

$$\dot{Q} = \varepsilon \cdot \dot{C} \cdot (T_{su} - T_w) \tag{29}$$

where $\dot{C} = \dot{M} \cdot c_p\left(p, \frac{T_{su}+T_{ex}}{2}\right)$; $\varepsilon = 1 - e^{-NTU}$ and $NTU = \frac{AU}{\dot{C}}$.

3.2.7 Closed volume

As stated above, the proposed heat exchanger models do not account for mass accumulation. Although this simplifies the equation system, it can also make the solution harder to find for the numerical solver since the flow rates are prescribed in all components. In order to ease the solution process, the *Volume* component has been developed, which can be considered as a high-level relaxation method for the solution process. This volume component is inserted between two components and can act as a mass damper by absorbing or rejecting a part of the flow. The practical experience when using the above models has shown that this component can significantly improve the solution process and the robustness of the models.

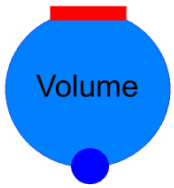

Figure 47: Icon of the *Volume* model

It should be noted that the volume component is also physically meaningful since it account for the dead volume of the piping between that components and for the internal volume of the heat exchangers.

It is modeled using the mass and energy conservation equations (1) and (4) already described in section 3.1.1 .

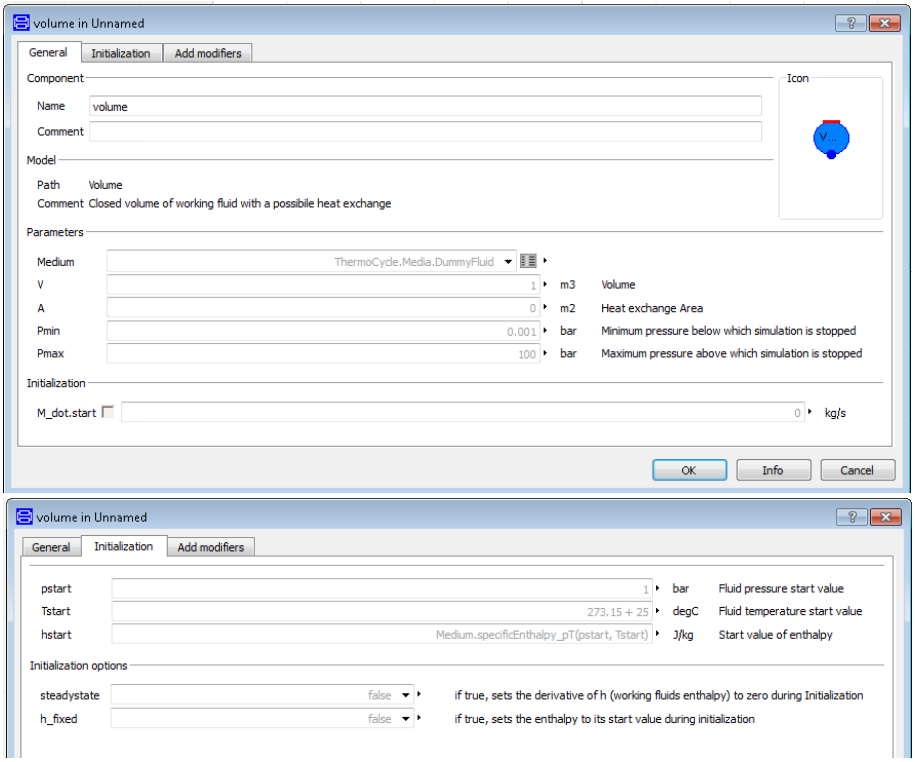

Figure 48: Parameters of the *Volume* model

3.2.8 Saturation state sensor

The *SensSat* model is a saturation state sensor for two-phase fluids, outputting the saturation temperature and pressure, as well as the vapor quality.

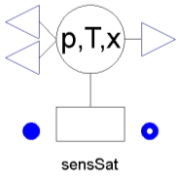

Figure 49: Icon of *SensSat*

This model has been created due to the need of controlling the vapor quality at the evaporator outlet in the boiler. It does not correspond to a physical device, but it is useful to set the evaporator pump speed in regard to the outlet vapor quality. It is also very useful to compute the turbine inlet superheating in case the latter is taken as control variable.

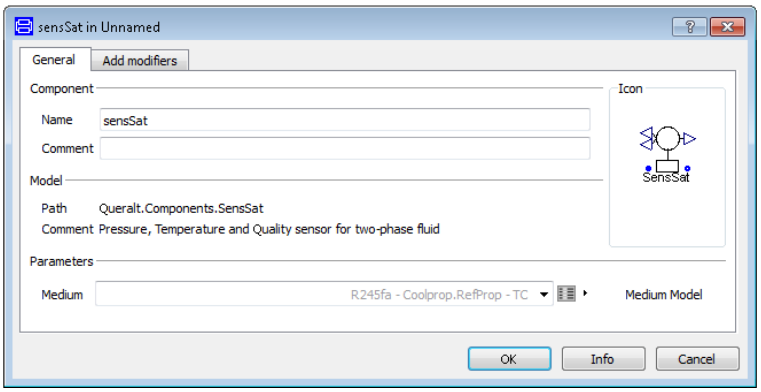

Figure 50: Parameters of *SensSat*

As shown in Figure 50, the medium model is left to the user, so the model can be used for different fluids.

3.2.9 Base components with (p,T) as state variables

In most Thermo-Flow models, the main variables describing the flow are the flow rate, the pressure and the enthalpy. Using the enthalpy ensures that no singularity will occur, even if the fluid is in two-phase state: a pair of inputs (p,h) allow to univocally define a thermodynamic state disregarding the fluid state at the point (liquid, two-phase or vapor).

However, for incompressible fluids in liquid state such as heat transfer fluids, two-phase flows are excluded and different input variables could be used. Most incompressible fluids properties are defined with polynomials or tables explicit in temperature. Hence, if enthalpy is used as an input, the solver has to numerically compute its value, which requires iterations on the temperature to find the desired

enthalpy. The idea is therefore to replace the (p,h) connectors by (p,T) connectors. This new flange connector that uses temperature as state variable is more computationally efficient and also avoids possible divergence or out-of-bounds errors caused by the numerical solver.

The connector is a stream connector (Franke et al., 2009) with *T_outflow* as the stream variable, which represents the temperature close to the connection point when the mass flow rate is going outside from the component. It has to be defined even if the mass flow rate is never supposed to leave the component.

Port (*Flange_pT*)

The *Flange_pT* is a port for single phase flows using pressure and temperature as state variables. Two connectors have been extended from the general one: an A-type (*FlangeA_pT*) and a B-type (*FlangeB_pT*) connectors. The two of them will be used as inlet and outlet connectors, respectively, in the models.

Flow rate source (*SourceMdot_pT*)

The *sourceMdot_pT* model is an ideal mass flow rate source for single phase flows with prescribed temperature of the fluid flowing from the model to the port (i.e.., out of the model). The port is a flange connector *Flange_pT*.

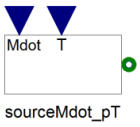

Figure 51: Icon of the flow rate source

As shown in Figure 51 and Figure 52, the mass flow rate and temperature can be set as parameters or defined by an input connector. It must be noticed that the boundary mass flow rate and temperature are imposed by the model only if the fluid is flowing out of the model. If flow reversal happens (i.e., mass flow rate flowing into the model) then the temperature is not imposed by the model.

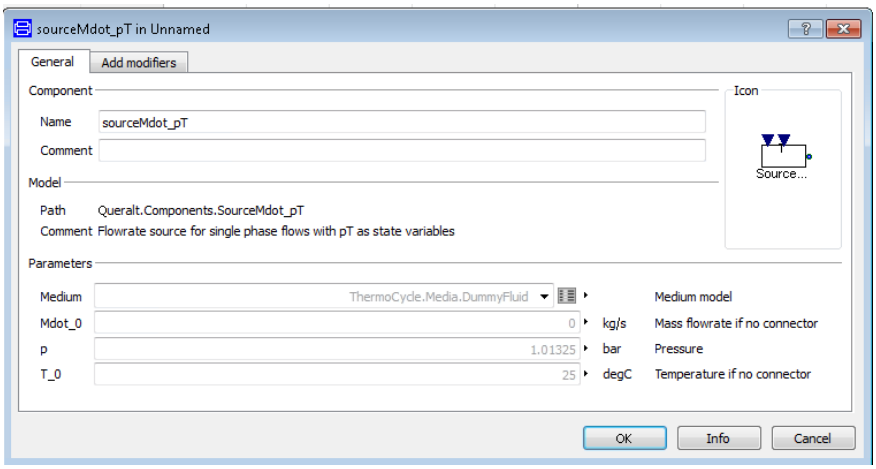

Figure 52: Parameters of the flow rate source

Pressure sink (*SinkP_pT*)

Model *sinkP_pT* is a pressure sink for single phase flows that sets the boundary pressure of the fluid from the port to the model (i.e., into the model). The port is a connector *Flange_pT* (pressure and temperature are used as state variables).

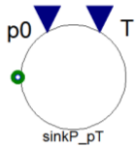

Figure 53: Icon of the pressure sink

As shown in Figure 53 and Figure 54, the pressure and temperature can be set as parameters or defined by an input connector. It must be noticed that boundary pressure is imposed by the model if the fluid is flowing into the model. If flow reversal happens (i.e. the mass flow rate is flowing out of the model) then the boundary temperature is also imposed by the model.

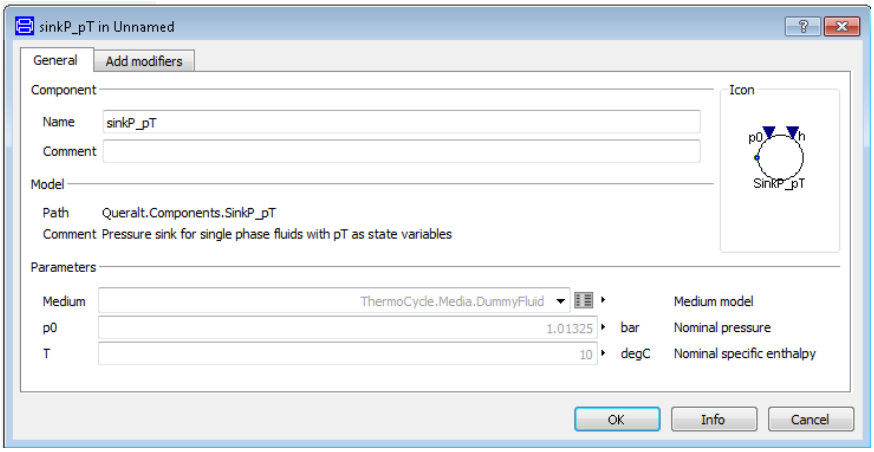

Figure 54: Parameters of the pressure sink

Flange converter

In order to ensure the compatibility of the pT connectors with the rest of the model and with the Modelica Standard Library (both using (p,h) as flow variables), a *FlangeConverter* model has been developed to convert the two types of ports.

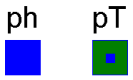

Figure 55: Icon of *FlangeConverter*

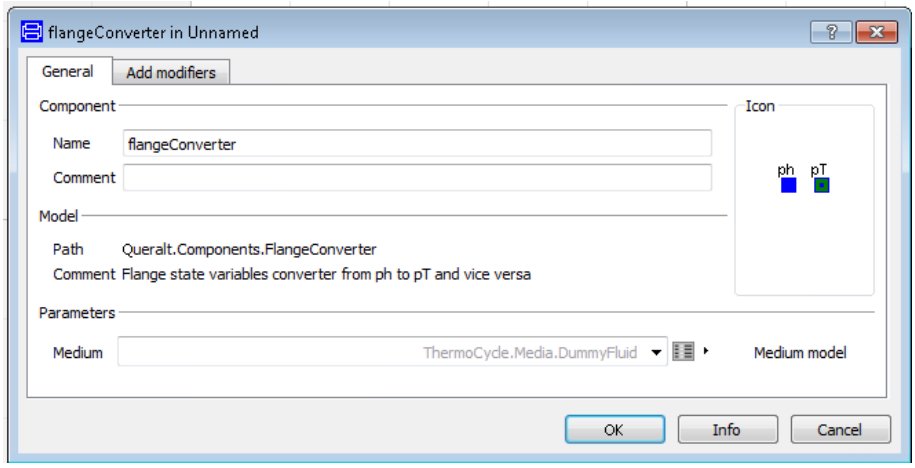

Figure 56: Parameters of the *flangeConverter* model

Chapter 4

CSP plant model

4.1 Boiler system

In order not to multiply the components in the overall cycle model, the boiler model has been built separately. Since the heat source characteristics from the CHP plant (i.e. high temperature flues gases) and from the CSP system (i.e. medium-temperature thermal oil) are different, the boiler has not been modeled as the one from the plant and has been simplified. The platen and the screen shown in Figure 5 (see chapter 2) have been removed, and the two evaporators and the four economizers have been merged to one economizer and one evaporator. Summarizing, as shown in Figure 58, the system subcomponents are: an economizer, an evaporator, two superheaters, a pump, two pressure drops and a drum.

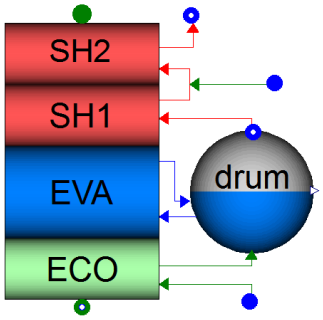

Figure 57: Icon of the boiler system

The economizer is modeled with the single-phase heat exchanger described in section 3.2.6. The inlet of the economizer is represented by a port, connected to the high pressure water coming from the feed water tank. This water is pre-heated in the economizer and undergoes a pressure before entering the drum. Since the heat exchanger model does not take into account the pressure drop, a separate model of it is inserted, as shown in Figure 58.

The liquid flow rate exiting the drum is imposed by the evaporator pump, whose speed is set in regard to the outlet vapor quality in the evaporator. For the purpose of the modeling, a saturation state sensor has been added to compute this quality, although

it does not correspond to any physical component. The evaporator is modeled with the two-phase heat exchanger detailed in section 3.2.6. As for the economizer, a pressure drop is added at the end of the evaporator, before its flow returns to the drum.

The vapor outflow of the drum is saturated vapor, which mainly goes to the superheater section, although a little fraction is used for the deaerator. The latter is represented by an outflow connector, whose flow rate can be regulated with a valve when building the overall model.

As in the CHP plant, the super-heater section is divided in two super-heaters, which are modeled with the single-phase heat exchanger described in section 3.2.6. As shown in Figure 58, there is the possibility of injecting liquid water into the flow before the second superheater. This is done to control the temperature of the vapor entering the high pressure turbine (after passing through this section). The outlet of the second superheater is represented by a connector. A pressure drop model must be added after this outlet when the model is used.

Finally, a real output is used to define the level of the water in the drum. This output is necessary for the control of the plant since the level of the drum and the speed of the feed pump are closely related.

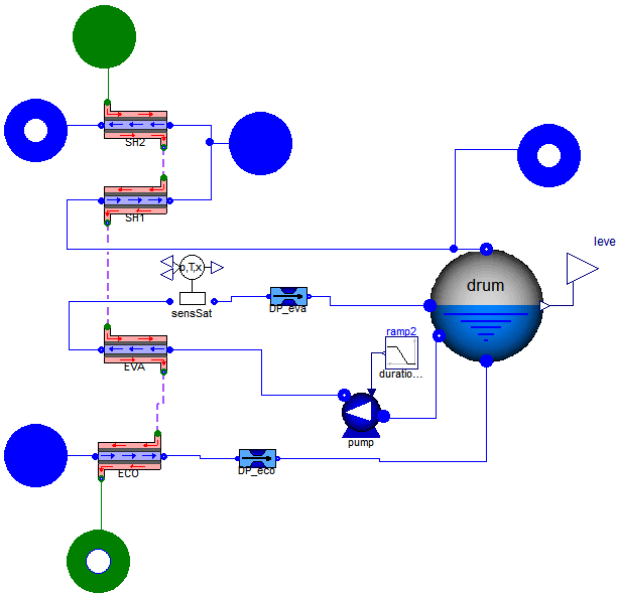

Figure 58: Diagram of the boiler system's subcomponents

Figure 58 is the detailed diagram of the boiler system, in which all the components appear interconnected. The secondary fluid of the boiler (i.e. heat transfer fluid coming from the parabolic troughs filed), enters at its maximum temperature in the superheaters, then flows through the evaporator and finally through the economizer. After leaving the economizer (i.e. it has been cooled and it is at its minimum temperature), the thermal oil is returned to the collectors to be heated up again.

Figure 59 shows the main parameters of the boiler system. To minimize the number of required user-inputs, the initialization temperature parameters of the four individual heat exchangers involved in the system are calculated with the initialization parameters defined in the overall boiler model. As an example, for the economizer outlet temperature of the secondary fluid, equation (30) is used:

$$T_{hf,eco,ex,start} = T_{sf,su,start} - \left(T_{sf,su,start} - T_{sat}(p_{start}) + pinch_{start}\right) \cdot \frac{6}{5} \qquad (30)$$

where $T_{hf,ex,start}$ is a parameter of the economizer model (i.e. single-phase heat exchanger), and $T_{sf,su,start}$, p_{start} and $pinch_{start}$ are parameters of the whole boiler system, as shown in Figure 59.

This equation is an approximation based on a pinch point calculation, but presents the advantage to provide a valid temperature profile as guess value of the Newton Solver with a limited number of user-defined start values.

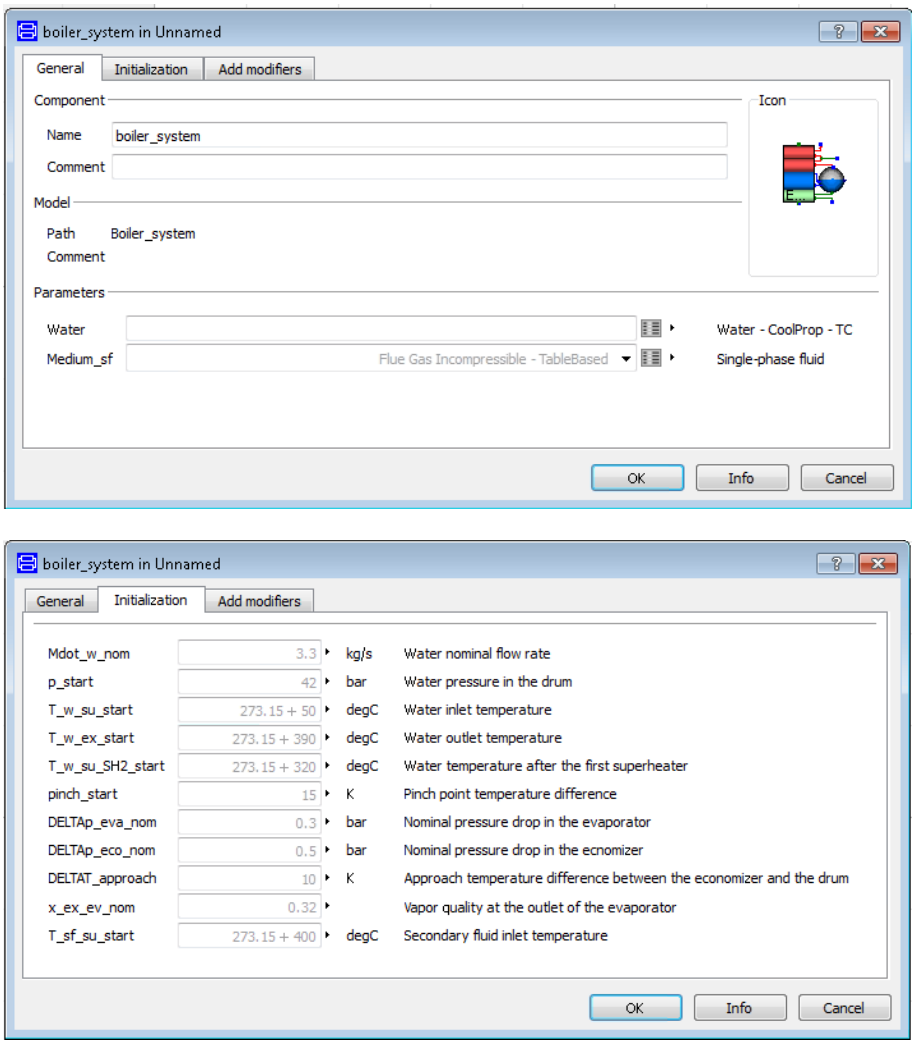

Figure 59: Parameters of the boiler system model

The values of the main parameters and modeling options of each sub-model of the boiler system are provided in Table 2:

Component	Tab	Parameter / Option	Value	Units
Drum	General	V	4	m^3
	Initialization	L_start	0.6	-
		impose_L	true	-
Pump	General	PumpInput	frequency	-
		eta_em	0.98	-
		eta_is	0.7	-
		epsilon_v	0.7	-
		V_dot_max	0.015	m^3/s
		use_constant_density	true	-
	Initialization	rhostart	1000	kg/m^3
dP_eco	General	UseNom	true	-
	Nominal Conditions	Mdot_nom	3.28	kg/s
		p_nom	42	bar
		T_nom	80	ºC
		rho_nom	1000	kg/m^3
		use_rho_nom	true	-
dP_eva	General	UseNom	true	-
	Nominal Conditions	use_rho_nom	true	-
ECO	General	M_wall	150	kg
		Cp_constant	false	-
		Use_AU	false	-
		A_cf	100	m^2
		A_hf	100	m^2
		U_cf	800	W/ m^2K
		U_hf	1000	W/ m^2K
	Initialization	steadystate_T_wall	false	-
		T_wall_fixed	true	-
EVA	General	M_wall	500	kg
		A_iso	150	m^2
		A_sf	150	m^2
		U_iso	2000	W/ m^2K
		U_sf	700	W/ m^2K
	Initialization	steadystate_T_wall	false	-
		T_wall_fixed	true	-
SH1	General	M_wall	300	kg
		Cp_constant	false	-
		Use_AU	false	-
		A_cf	15	m^2
		A_hf	15	m^2
		U_cf	1000	W/ m^2K
		U_hf	1000	W/ m^2K
	Initialization	steadystate_T_wall	false	-
		T_wall_fixed	true	-
SH2	General	M_wall	200	kg
		Cp_constant	false	-
		Use_AU	false	-
		A_cf	15	m^2
		A_hf	15	m^2
		U_cf	600	W/ m^2K

Component	Tab	Parameter / Option	Value	Units
		U_hf	800	W/ m^2K
	Initialization	steadystate_T_wall	false	-
		T_wall_fixed	true	-

Table 2: Parameters of the boiler model

4.2 Overall cycle model

After the development of each subcomponent model, a dynamic model of the overall cycle is built for the purpose of evaluating the system's reaction to transient conditions. The model consists in a steam cycle coupled to a parabolic troughs model.

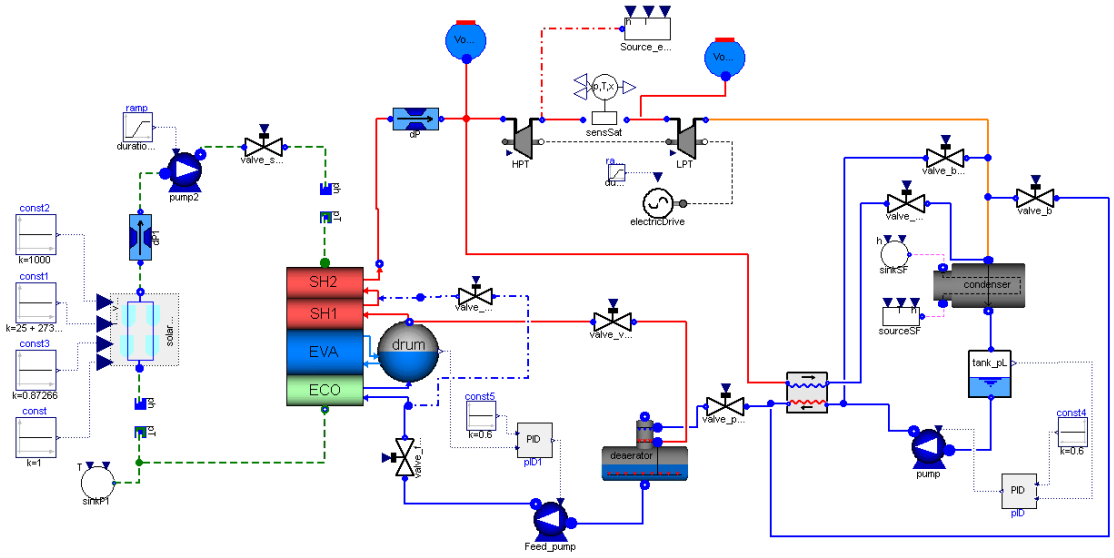

Figure 60: Overall cycle model diagram

Turbines

As previously stated, the steam cycle is based on the biomass CHP plant available on the University campus in Sart-Tilman (Liège, Belgium). Firstly, two turbines are connected consecutively. The first one works at a high pressure and the second one at a low pressure. All the fluid that flows through the high pressure turbine flows through the low pressure one, i.e. there is no steam extraction between them. However, the model offers this possibility.

In reality, there is a pipe volume from one turbine to the other, i.e. the mass flow rate going out of the high pressure turbine does not have to be equal to the mass flow rate going into the low pressure turbine. Because of a possible mismatch between the two turbine flow rates, some potentially problems can appear during the initialization phase. Therefore, as shown in Figure 60, the *Volume* component has been interconnected between them, and acts as a mass damper by absorbing or rejecting a part of the flow. This component can be seen as that dead volume of the piping between the turbines.

The inlet temperature at the high pressure turbine is lower than that of the CHP plant because of the different heat source characteristics between the CHP and the CSP systems (high temperature flues gases vs. medium-temperature thermal oil). Therefore, the nominal conditions at the turbine inlet are quite different in the CSP system compared to the reference CHP plant (Table 1).

The turbines are connected to a generator model, which computes the total electrical power generated.

Condenser

The flow going out of the second turbine is the main inlet of the condenser, although the latter also has three more entering flows. The main condenser model parameters are the global heat exchange area, the fluid volume and the wall mass. As explained in section 3.2.2, it is assumed that the *n* U-tubes can be represented by one straight-tube with the equivalent heat exchange area and fluid volume. Consequently, these parameters are computed with the given data from Table 1:

$$A_{wf} = n_{tubes} \cdot \pi \cdot D_o \cdot L \; ; \; A_{sf} = n_{tubes} \cdot \pi \cdot D_i \cdot L \; ; V_{sf} = n_{tubes} \cdot \frac{\pi}{4} \cdot {D_i}^2 \cdot L \qquad (31)$$

$$M_w = n_{tubes} \cdot \frac{\pi}{4} \cdot \left({D_o}^2 - {D_i}^2\right) \cdot L \cdot \rho_w \qquad (32)$$

For the metal wall, the density used is $\rho_w = 7.86 \; g/cm^3$ and the specific heat capacity is set to $500 \; J/(kg \cdot K)$.

The secondary fluid from the CHP plant is a 40% propylene glycol (Table 1). For the model, a similar fluid already available in the Modelica library has been used: a propylene glycol mixture with water, whose concentration is 47%. The pipe has been discretized in 5 cells, which lead to a good agreement between accuracy and computation speed.

No information was available about the heat transfer coefficients for both working and secondary fluid. Therefore, some correlations proposed in (Nellis and Klein, 2009) have been used to compute an approximate value:

- For the secondary fluid, which experiences convection with the metal wall, the correlation returns the average heat transfer coefficient for a specified mass flow rate through a circular tube of diameter D and length L, and whose concentration of the propylene-glycol with water is provided in %. The procedure is presented in section 5.2.4 of (Nellis and Klein, 2009).
- For the working fluid, which experiences condensation on the metal wall, the correlation calculates the heat transfer coefficient for condensation on a bank of

N horizontal cylinders in quiescent saturated vapor, where N is the number of cylinders in the vertical direction. The procedure was previously presented in section 7.4 of (Kakaç et al., 1997), but is also described in section 6.4.3 of (Nellis and Klein, 2009).

It should be noted that the newly developed *crossCondenser* component is not sufficient to represent a physical condenser because it does not consider the condensed steam flow collected at the bottom of the condenser. Therefore, the *tank_pL* model already available in the ThermoCycle library has been added after it. This component allows computing the working pressure of the condenser. It acts as a natural pressure controller with feedback, which can be illustrated in the case where the condensing pressure decreases:

Condensing pressure increases
⇒ Average temperature differences in the condenser increases
⇒ Heat transfer increases
⇒ The working fluid is "too condensed" and exits in a subcooled liquid state
⇒ This cold flow in the liquid receiver causes a part of the steam to condense
⇒ The pressure decreases

There is therefore an auto-regulating effect that is also valid in case of pressure increases perturbation.

In reality, the volume of the water condensed at the bottom of the condenser is small compared to the volume of the condenser shell. Therefore, the volume set for the *tank_pL* has been assumed to be much smaller than the volume of the working fluid's shell in the condenser.

Pump

After the *tank_pL*, there is a pump that extracts the condensed steam and circulates it to the preheater. However, before entering the latter, a portion of this flow is returned to the inlet of the condenser. The mass flow rate of this portion is defined by a liner valve called "valve_b".

Because no data of the pump was available, the parameters have been set to typical values such as an electro-mechanical efficiency of 98% and an internal isentropic efficiency and a volumetric effectiveness of 70%.

The pump speed is regulated by a control system (described in chapter 5), which acts on the pump frequency, in order to avoid filling or emptying the tank. The maximum volumetric flow rate has been set to a value sufficient to ensure a good control of the liquid level in most operating conditions.

Preheater

As previously mentioned, the cold fluid of the preheater is the water from the condenser pump. This water will be heated up while receiving heat from the hot fluid. The latter is a portion of super-heated steam extracted between the second super-heater and the high pressure turbine or between the two turbines. Its flow rate is regulated by a linear valve (called “valve_wf_preheater”), adjusted in such a way that the fluid is fully condensed.

The model has been discretized into 10 cells and only one tube in parallel is considered. Since no data of the geometry or the heat transfer was provided, the parameters have been set to typical values, and then manually adjusted based on the steady-state model of the CHP plant nominal conditions (Sartor et al., 2014).

Deaerator

The boiler feed water from the preheater is then sent to the deaerator. It must be taken into account that some non-condensable gases can appear during the condensation process of the steam in the condenser, due to the low working pressure. These gases are not modeled, but are supposed to be separated from the water in the deaerator, as already explained in section 3.2.5. The steam used for that purpose comes from the drum in the boiler system. Its flow rate and pressure drop is adjusted by a valve (called “valve_vapor_vs_deaerator”). It should also be noted that in this work, no distinction is made between the deaerator and the feed water tank, although in practice they can be separate components.

Feed pump

The water stored in the deaerator vessel is then pumped to the boiler system by the feed pump. Because no data of the pump was available, the parameters have been set to typical values such as an electro-mechanical efficiency of 98%, an internal isentropic efficiency of 80% and a volumetric effectiveness of 70%.

As for the condenser pump, the pump speed is regulated by a control system (described in chapter 5), to control the liquid level in the drum.

Boiler

For the purpose of this work, the secondary fluid chosen for the boiler, i.e. the fluid flowing through the collector’s absorber pipe is a synthetic heat transfer fluid called

Therminol VP-1. It has an efficient, uniform performance in term of transport properties in a wide optimum range of 12ºC to 400ºC. It also presents the highest thermal stability temperature of all organic heat transfer fluids. Therminol VP-1 is already available in ThermoCycle library. Its properties are computed with CoolProp.

Solar system

The size of the parabolic troughs field was selected to provide the right heat flow to the steam cycle (whose size was determined by the CHP plant at Sart Tilman). The parabolic troughs have been divided in 18 cells.

Since the pressure is considered constant in the solar field model, a pressure drop model has been added at the outlet. The pump model combined with the pressure drop model allows setting the pressure difference in the thermal oil loop. However, the absolute pressure levels still need to be fixed. Therefore, a *sinkP_pT* model is added to the loop to fix one of the two pressure levels.

The values of the main parameters and modeling options of each sub-model interconnected in the overall cycle model are provided in Table 3:

Component	Tab	Parameter / Option	Value	Units
HPT	General	eta_mech	0.98	-
		eta_s_nom	0.6942	-
		UseNom	true	-
		use_ideal_gas	true	-
	Initialization	p_su_start	35.3	bar
		p_ex_start	3.15	bar
		M_dot_start	3.27	kg/s
		h_su_start	3.027e6	J/kg
		h_ex_start	2.692e6	J/kg
	Nominal Conditions	M_dot_nom	3.01	kg/s
		p_su_nom	33.4	bar
		p_ex_nom	2.95	bar
		T_nom	351.85	ºC
LPT	General	eta_mech	0.98	-
		eta_s_nom	0.7	-
		UseNom	true	-
		use_ideal_gas	true	-
	Initialization	p_su_start	3.15	bar
		p_ex_start	0.168	bar
		M_dot_start	3.27	kg/s
		h_su_start	2.692e6	J/kg
		h_ex_start	2.381e6	J/kg
	Nominal Conditions	M_dot_nom	3.01	kg/s
		p_su_nom	2.95	bar
		p_ex_nom	0.145	bar

Component	Tab	Parameter / Option	Value	Units
		T_nom	147.35	ºC
Volume	General	V	1	m^3
	Initialization	pstart	3.01	bar
		Tstart	131	ºC
		steasystate	false	-
		h_fixed	false	-
Cross Condenser	General	Medium2	1,2 propylene glycol 47%	
		N	5	-
		A_wf	279.61	m^2
		A_sf	252.09	m^2
		V_sf	1.5	m^3
		Mdotnom_sf	585 176 / 3600	kg/s
		M_wall_tot	2 552.13	kg
		c_wall	500	J/kgK
		Medium2Heat TransferModel	Mass Flow Dependence	
		Unom_sf	769	W/m^2K
		U_wf	9250	W/m^2K
	Initialization	Tstart_sf_in	12.69	ºC
		Tstart_sf_out	21.95	ºC
		T_sat_start	56.34	ºC
		h_su_wf_start	2.053e6	J/kg
		h_ex_wf_start	2.36e5	J/kg
		T_start_wall	53.5	ºC
		steadystate_sf	true	-
		steadystate_T_w	false	-
	Numerical Options	Discretization_sf	upwind_AllowFlowReversal	
Tank_pL	General	Vtot	1	m^3
	Initialization	pstart	0.168	bar
		L_start	0.6	-
		impose_L	false	-
		impose_p	false	-
Pump	General	PumpInput	frequency	-
		eta_em	0.98	-
		eta_is	0.7	-
		epsilon_v	0.7	-
		V_dot_max	1.5*5.134e-3	m^3/s
		use_constant_density	true	-
	Initialization	M_dot_start	2.635	kg/s
		hstart	1.81e5	J/kg
		rhostart	986	kg/m^3
Preheater	General	N	10	-
		A_sf	3.3	m^2
		A_wf	3.3	m^2
		counterCurrent	true	
		Mdotnom_sf	11 450 / 3600	kg/s
		Mdotnom_wf	130 / 3600	kg/s
		Medium2Heat TransferModel	MassFlowDependence	
		Unom_sf	1071	W/m^2K
		Medium1Heat TransferModel	MassFlowDependence	
		Unom_l	769.8	W/m^2K

Component	Tab	Parameter / Option	Value	Units
		Unom_tp	6015	W/m^2K
		Unom_v	400	W/m^2K
	Initialization	pstart_sf	9.8	bar
		pstrart_wf	0.9	bar
		Tstart_inlet_wf	103.61	ºC
		Tstart_outlet_wf	64.89	ºC
		Tstart_inlet_sf	56.62	ºC
		Tstart_outlet_sf	62.01	ºC
		steadystate_T_sf	false	-
		steadystate_h_wf	false	-
		steadystate_T_wall	false	-
	Numerical Options	Discretization	upwind_AllowFlowReversal	
		Mdotconst_wf	true	-
Valve_ bypass	General	UseNom	true	-
		Xopen	1	-
		CheckValve	true	-
	Nominal Conditions	Mdot_nom	0.222	kg/s
		DELTAp_nom	7.65	bar
Valve_b	General	UseNom	true	-
		Xopen	1	-
		CheckValve	true	-
	Nominal Conditions	Mdot_nom	0.225	kg/s
		DELTAp_nom	7.65	bar
Valve_ preheater_ vs_ deaerator	General	UseNom	true	-
		Xopen	1	-
		CheckValve	true	-
	Nominal Conditions	Mdot_nom	2.93036	kg/s
		DELTAp_nom	7.57	bar
Deaerator	General	Vtot	10	m^3
	Initialization	pstart	1.286	bar
		L_start	0.212	-
		impose_L	false	-
		impose_pressure	false	-
Feed pump	General	PumpInput	frequency	-
		eta_em	0.98	-
		eta_is	0.8	-
		epsilon_v	0.7	-
		V_dot_max	1.2*5.39e-3	m^3/s
		use_constant_density	true	-
	Initialization	M_dot_start	2.8429	kg/s
		hstart	4.615e5	J/kg
		rhostart	950	kg/m^3
Valve_feed _water	General	UseNom	true	-
		Xopen	1	-
		CheckValve	true	-
	Nominal Conditions	Mdot_nom	2.8430	kg/s
		DELTAp_nom	0.5	bar
Boiler system	Initialization	Mdot_w_nom	2.9	kg/s
		p_start	36.35	bar
		T_w_su_start	107.12	ºC
		T_w_ex_start	353.85	ºC
		T_w_su_SH2_start	320.35	ºC
		pinch_start	25	K

Component	Tab	Parameter / Option	Value	Units
		DELTAp_eva_nom	0.3	bar
		DELTAp_eco_nom	0.5	bar
		DELTAT_approach	1	K
		x_ex_eva_nom	0.307	-
		T_sf_su_start	380	ºC
dP	General	UseNom	true	-
	Nominal Conditions	Mdot_nom	3.0339	kg/s
		p_nom	34.3	bar
		T_nom	370	ºC
		DELTAp_lin_nom	1.009	bar
		use_rho_nom	true	-
Volume2	General	V	1	m^3
	Initialization	pstart	32.4	bar
		Tstart	320	ºC
		steadystate	false	-
		h_fixed	false	-
Valve_ vapor_ deaerator	General	UseNom	true	-
		Xopen	1	-
		CheckValve	true	-
	Nominal Conditions	Mdot_nom	0.206	kg/s
		DELTAp_nom	27.6	bar
sourceSF (condenser)	General	Medium	1,2-propylene glycol 47%	
		Mdot_0	585 176 / 3600	kg/s
		p	2.48	bar
		UseT	true	-
		T_0	10	ºC
sinkSF (condenser)	General	Medium	1,2-propylene glycol 47%	
		p0	2.48	bar
solarField_ Forristal_Inc	General	N	2	-
		Ns	9	-
		Nt	30	-
		L	16	m
		A_P	5	m
		Mdotnom	25	kg/s
		Unom	1000	W/m^2K
		HeatTransferModel	MassFlowDependence	
	Initialization	Tstart_inlet	200	ºC
		Tstart_outlet	400	ºC
		pstart	20	bar
	Numerical Options	Discretization	upwind_AllowFlowReversal	
dP1 (solar)	General	UseNom	true	-
		DELTAp_0	5	
	Nominal Conditions	Mdot_nom	25	kg/s
		p_nom	25	bar
		T_nom	380	ºC
		rho_nom	900	kg/m^3
		DELTAp_quad_nom	5	bar
		use_rho_nom	false	-
	Initialization	DELTAp_start	5	bar
Pump2 (solar)	General	PumpInput	frequency	-
		eta_em	0.98	-
		eta_is	0.7	-
		epsilon_v	0.7	-

Component	Tab	Parameter / Option	Value	Units
		V_dot_max	0.0494	m^3/s
		use_constant_density	true	-
	Initialization	M_dot_start	25	kg/s
		hstart	3e5	J/kg
Valve_solar	General	UseNom	true	-
		Xopen	1	-
		CheckValve	true	-
	Nominal Conditions	Mdot_nom	25	kg/s
		DELTAp_nom	0.1	bar
sinkP (solar)	General	p0	20	bar

Table 3: Parameters of the overall cycle model

4.3 Thermo-physical properties of the working fluids

As already stated, the models are implemented in the Modelica language and the fluid properties are computed using CoolProp (Bell et al., 2014). The interface between CoolProp and Modelica is based on the CoolProp2Modelica library (Quoilin et al., 2014b), which is a modified version of the ExternalMedia library (Ritcher and Casella, 2008).

The working fluid is defined as a package in the core of the overall model. Figure 61 shows an example of such definition: the working fluid (Water) is defined with density smoothing (see section 4.3.1), the TTSE method (see section 4.3.2) enabled and a debug verbosity level of 0.

```
package Water "Water - CoolProp - TC"
  extends CoolProp2Modelica.Interfaces.CoolPropMedium(
    mediumName = "water",
    substanceNames = {"water|rho_smoothing_xend=0.1|enable_TTSE=1|debug=0"},
    ThermoStates=Modelica.Media.Interfaces.PartialMedium.Choices.IndependentVariables.ph);
end Water;
```

Figure 61: Definition of the working fluid in the overall model

4.3.1 Integration of the thermo-physical properties: TTSE method

The computation of the thermodynamic states usually involves equations of state explicit in temperature and density, whereas the state variables used in this work are pressure and enthalpy. Therefore, the solver has to iterate on the equation to compute the state variables, which is time consuming and leads to a slower simulation. There are several interpolation methods that can be used to compute the thermodynamic properties of the working fluid (e.g. 2-D spline, TTSE). In this work, the Tabulated Taylor Series Expansion (TTSE) method is used. The main characteristics of this method are (ThermoCycle, 2014):

- At every grid point, the EOS is used to compute the property and its derivatives with respect to the state variables.

- A second order taylor approximation is used between two grid points:

$$T = T_{i,j} + \Delta h \left(\frac{\partial T}{\partial h}\right)_p + \Delta p \left(\frac{\partial T}{\partial p}\right)_h + \frac{\Delta h^2}{2}\left(\frac{\partial^2 T}{\partial h^2}\right)_p + \frac{\Delta p^2}{2}\left(\frac{\partial^2 T}{\partial p^2}\right)_h + \Delta h \Delta p \left(\frac{\partial^2 T}{\partial p \partial h}\right) \quad (33)$$

This method is faster than applying a 2-D spline but generate discontinuities at the junction between two TTSE interpolations. However, the discontinuities are very small (usually smaller than the solver tolerance) and do not constitute an issue in the present model.

The process consists in building an interpolation table with the fluid properties at the first property call, cache it and then re-use it for the following property calls, and requires between 2 and 10 seconds. It has been proven that methods such as the TTSE can decrease the computational time of a property call up to 20 times and the computation time of a complex model involving many property calls up to 5 to 10 times. Nevertheless, TTSE is an approximation method and therefore brings an error to the results. Figure 62 however shows that this error is negligible for most of the T-s diagram plane.

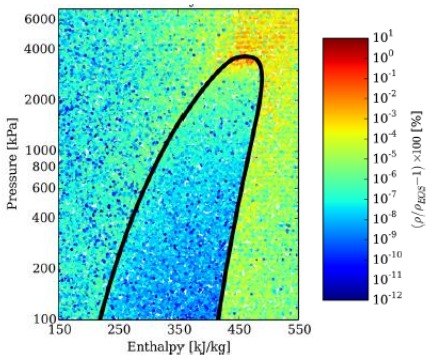

Figure 62: Error in density from TTSE (Bell et al., 2014)

A simple flag in when passing the working fluid name to the library is enough to activate the method.

4.3.2 Avoiding chattering and flow-reversals: density smoothing

The chattering phenomena may appear when the model variables have discontinuities and can lead to extremely slow simulation or to simulation failures. In discretized two-phase models, the main discontinuity is usually the density derivate on the liquid saturation curve. In the model of the steam plant, there is only one discretized heat exchanger undergoing a two-phase flow, i.e. the preheater. Since this heat exchanger is subject to chattering and flow reversals, methods had to be implemented to deal with it.

In (Quoilin et al., 2014a) several solutions are presented to avoid numerical flow reversals, which are implemented in CoolProp. In this work, the density smoothing method is used. As shown in Figure 63, the process smoothes out the density (i.e. makes it C1-continuous using a spline function) for a range of vapor qualities and recalculates its partial derivates in the smoothed area. The density derivates are therefore continuous, but not smooth.

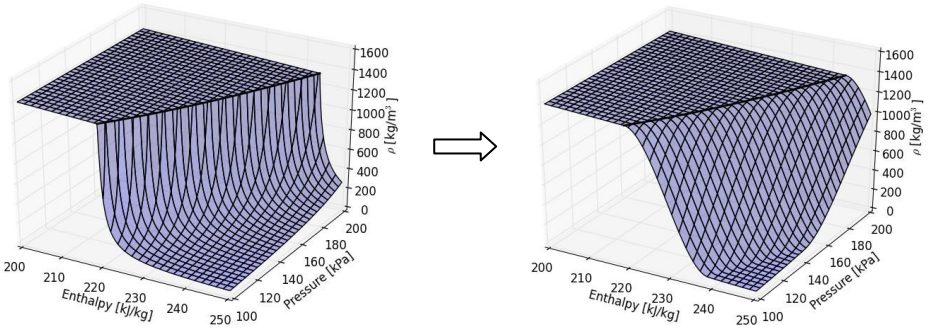

Figure 63: Density vs. pressure and enthalpy (original and smoothed) (ThermoCycle, 2014)

A simple flag in when passing the working fluid name to the library is enough to activate the method.

4.3.3 Incompressible fluids

The properties of incompressible fluids such as heat transfer fluids are usually defined with polynomials or tables explicit in temperature. It is this work, the incompressible fluid is the heat transfer fluid Therminol VP-1, whose properties are calculated based on the polynomials provided in (SOLUTIA, 2014). An example of such polynomial is provided below, describing the evolution of the heat capacity with the temperature:

$$Cp = 1.498 + 0.002414 \cdot T + 5.9591 \cdot 10^{-6} \cdot T^2 - 2.9879 \cdot 10^{-8} \cdot T^3 + 4.4172 \cdot 10^{-11} \cdot T^4 \quad (34)$$

where the heat capacity Cp is in kJ/kgK and the temperature T in ºC.

Integrating the above equation, it is quite straightforward to compute the fluid enthalpy h(p,T) as a function of the temperature and of the pressure. However, for polynomials orders higher than 2, it is not possible to find a analytical equation providing the temperature as a function of enthalpy and pressure T(h,p). In this case, a numerical method must be used. The one implemented in Coolprop is the secant method, and is used whenever an incompressible fluid is defined with h and p as state variables.

Chapter 5

Control of the plant

Controlling a complete CSP steam power plant is quite a complex task due to the multiplicity of control variables and measurements. The main control variables are typically the pump speeds and the valve openings. In this work, a simple control system has been defined based on the liquid levels in the drums.

Three water storage vessels can be found in the cycle: the condenser (i.e. represented by the *tank_pL*), the deaerator and the boiler's drum. It should be noted that these components together with the *Volume* components are the only ones where mass accumulation occurs since heat exchanger models assume equal inlet/outlet flows.

From these vessels, the water is pumped to another part of the system. The speed of the pump is therefore an important parameter because in transient conditions, the levels can vary quickly, and the pump speeds have to be adjusted in order to maintain stable that levels. As shown in Figure 60, two control systems have been implemented: one for the pump after the condenser and another for the feed pump (i.e. after the deaerator and before the boiler drum). Two controllers are sufficient for the three two-phase tanks because, the total working fluid mass in the system being constant, the level in the third tank is a result of the levels in the two other tanks. The mass in the *Volumes* components is neglected since they only contain low-density steam.

To adjust the delivered flow rate, the control signals are either the pump frequency or either the pump flow fraction, the choice being left to the user (section 3.1.2). In this work, the control signal is the pump frequency, assumed to vary in a 0 to 50 Hz range. The controlled signals (or "Present Values") are the relative levels of the condenser receiver, and of the boiler drum, both with a set point of 60%.

The control system used is the *PID* model, already available in ThermoCycle. The PI controller has been chosen over the PID controller due to its lower sensitivity to measurement noise. Furthermore, PI controllers have a good behavior in simulations and are proved to be able to maintain the desired working conditions. The control signal of the controller is described by the equation:

$$CS(t) = CS_0 + K_p \cdot \left(e(t) + \frac{1}{\tau_I} \cdot \int_0^t e(t)dt \right) \quad (35)$$

where $K_p$is the gain, $\tau_I$the integral time and $e(t)$ the error term (i.e. the difference between the present value and the set point).

In addition, the *PID* model has a tracking signal for anti-windup integral action. The proportional gain parameter K_p and the integral time parameter τ_I have to be properly defined in order to ensure a proper control, suitable over a wide range of working conditions. Increasing K_p tends to make the response faster, although if it is too large an undesirable degree of oscillation can appear. Decreasing τ_I tends to make the response faster but can also results in excessive overshoots.

Figure 64 and Figure 65 show the variability of the response for different values of the parameters. The *red colored* control, which has a higher K_p and a lower τ_I, is much more efficient than the *blue* one. The process response turns out to be extremely fast: the number of oscillations decreases and the deviation between the level and the set point becomes much smaller.

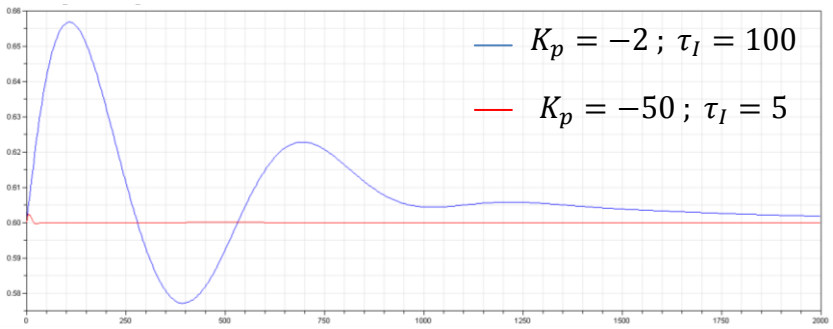

Figure 64: Level of the *tank_pL*

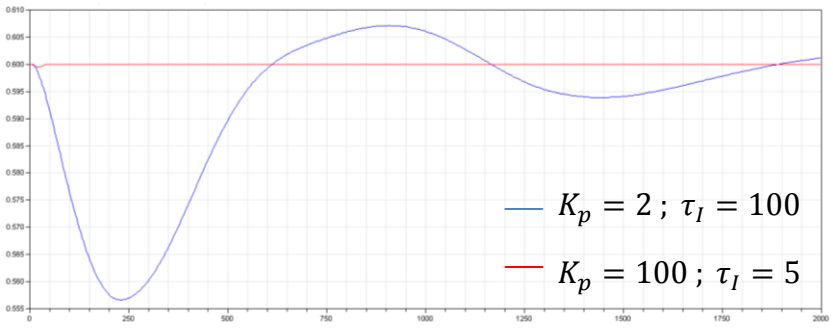

Figure 65: Level of the boiler's drum

The main lesson learned from the tuning of the PI controllers is that the liquid levels are relatively easily-controlled variables: a simple manual tuning proved to give excellent results. This is due to the fast response between a variation of the pump speed and the level in the tank compared to the slower process of liquid condensation/evaporation, which is linked to slower thermal and pressure variables.

Chapter 6

Simulation results

Several simulations of the model have been performed in order to test the developed library of models. It should be noted that these simulations do not focus on the value of the results (e.g. efficiencies) since the modeled system and selected parameters are very hypothetical. The main goal is to evaluate how the models react in different situations, such as transient conditions (e.g. varying the irradiation data) or cycle configuration (e.g. different positions of the steam extraction). The robustness and computational efficiency of the models, which are the main focus of this work, will be also evaluated.

The preliminary simulation is intended to be simple in order to compute general steady-state results (e.g. see the pressure levels, the temperature profiles, efficiency of the cycle, etc.). Therefore, the model inputs have been set to constant values, as shown in Table 4:

Component	Real Input	Value	Units
SolarField_Forristal	DNI	1 000	W/m^2
	v_wind	1	m/s
	Theta	0.87266	rad
	T_ambient	25	ºC
Pump2 (solar side)	frequency	40	Hz
Pump (condenser)	frequency	*PID*	-
Feed pump	frequency	*PID*	-
Pump (evaporator)	frequency	50	Hz
Valve_wf_to_preheater	Opening	5	-

Table 4: Real Inputs of the overall cycle model

The simulation lasts 4000s. To display the results, the ThermoCycle Viewer has been used. This software provides an animation of the temperature profiles in discretized models (i.e. one dot per cell) and the thermodynamic states, which is very useful to interpret the simulation results. However, ThermoCycle Viewer was designed to display discretized temperature profiles only. Furthermore, it only displays the profile of one heat exchanger at a time. In the present case, it would be interesting to obtain

the temperature profiles of the four heat exchangers in the same plot, to see the evolution of the working fluid through the whole boiler system. Therefore, the code of the ThermoCycle Viewer has been modified. The new version plots the nodes of the heat exchangers versus the heat power, as shown in Figure 66.

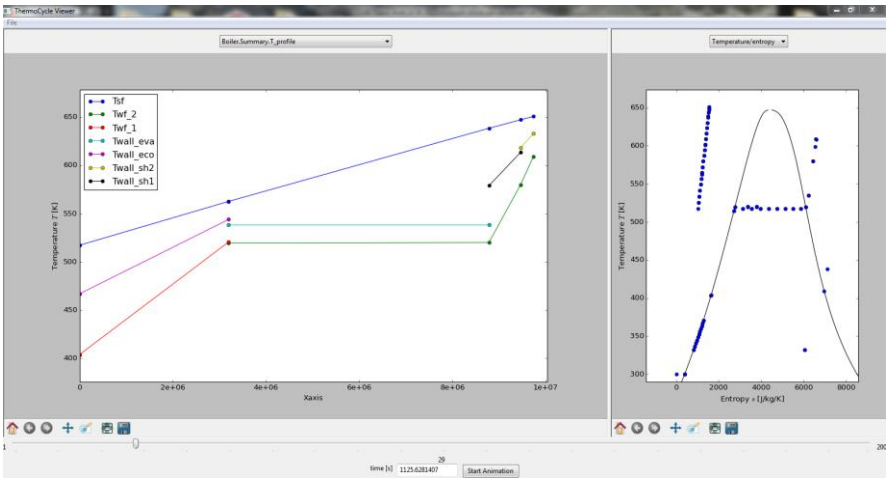

Figure 66: Screenshot of the main windows of ThermoCycle Viewer, showing the temperature profile in the boiler (left) and the detected thermodynamic states (right)

As shown in the Temperature-Entropy diagram of Figure 66, there are four main pressure levels:

- The boiler, high pressure turbine inlet and working fluid side in the preheater
- The secondary fluid side in the preheater
- The deaerator
- The condenser

The computed thermal efficiency is about 22,3% for the steam cycle and 46,4% for the collectors. The overall efficiency is around 10,3%. This efficiency is relatively lower than that of typical CSP systems of the same size. As a comparison the Andasol plant shows a steam cycle efficiency of 37.5% and a collector efficiency of 66%, for an overall efficiency of 25% in peak conditions and 14.7% annually (Herrmann et al., 2002). This lower efficiency is explained by the following factors:

- The steam cycle taken as reference (the CHP plant at Sart-Tilman) presents a very low efficiency (see Table 1) and a non-optimal cycle architecture
- The collectors taken as reference correspond to the Californian SEGs plants, which are about 30 years old. The new generation of collectors, such as the one used in the Andasol project, present a higher efficiency.
- The design of the whole plant has not been optimized: parameters such as the boiler pressure or the component sizes could be optimized with respect to the cycle boundary conditions.

In addition, as previously stated, the model does not focus on maximizing the cycle performance, but on testing the component models in different situations. To aim that, four different simulations have been performed:

- **Simulation 1**: Varying the DNI
- **Simulation 2**: Varying the working fluid flow rate in the preheater
- **Simulation 3**: Changing the position of the steam extraction
- **Simulation 4**: Varying the mass flow rate in the evaporator

6.1 Simulation 1: Varying the DNI

The first simulation consists in varying the solar irradiation data in order to represent a real case, e.g. a cloud that sudden blocks the sun, to see the reaction of the system. The irradiation, input of the solar filed model, has been defined as a step that varies from 1000 W/m^2 to 500 W/m^2 at 5000s (i.e. after a steady-state has been obtained).

The temperature at the outlet of the collectors decreases from approximately 385ºC to 275ºC. The output power is reduced from 2,2MW to 1,1MW. It should be noted that a control system could be implemented to regulate the collector outlet temperature by adjusting the pump speed, in order to optimize the efficiency. However, this simulation does not focus on the efficiency of the cycle, but on the response time and the delay of the reactions in different parts of the cycle, such as the superheating temperature, the pressure in the boiler, the electrical power and the condensing pressure.

In order to compare the magnitude of the delays, these variables have been converted into adimensional ones (i.e., their values move between 0 and 1), as shown in Figure 67.

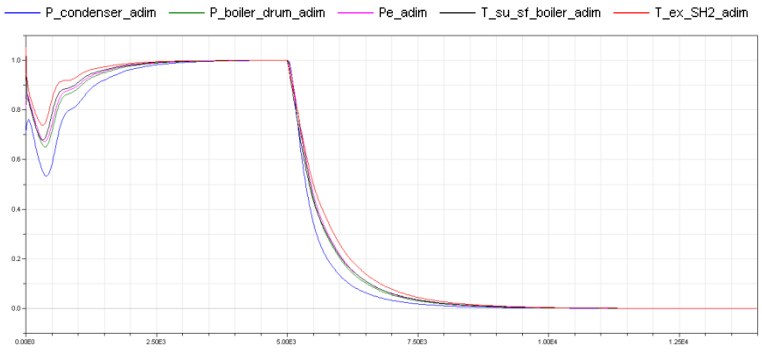

Figure 67: Adimensional plot

The upper plot of Figure 68 shows that there is a delay in the response of the variables from the system after the step. The delays are different depending on the type and the situation of the considered variable. As shown in Figure 68, just after the step, the reaction time of the different variables are ordered in the following manner (from the fastest to the slowest):

1. $T_{su,sf,boiler,adim}$
2. $T_{ex,wf,SH2,adim}$
3. Pe_{adim}
4. $P_{boiler,drum,adim}$
5. $P_{condenser,adim}$

However, after a certain simulation time (about 500 to 1000s), this order is modified and becomes:

1. $P_{condenser,adim}$
2. $P_{boiler,drum,adim}$
3. Pe_{adim}
4. $T_{su,sf,boiler,adim}$
5. $T_{ex,wf,SH2,adim}$

This phenomenon can be explained in the following way: just after the step, the response time of the different variables is explained by a "proximity parameter". The heat transferred to the oil decreases, so the temperature at the outlet of the collectors (i.e. *T_su_sf_boiler_adim*) is the first affected variable. The following effects are in the boiler. The super-heating outlet temperature (i.e. *T_ex_SH2_adim*) is the second affected, because it depends on the inlet temperature of the oil in the boiler. The boiler's pressure (i.e. *P_boiler_drum_adim*), will also decrease, and with it, the boiler mass flow rate. With a lower super-heating temperature of the fluid flowing through the turbines and a lower flow rate, the electrical power (i.e. *Pe_adim*) becomes smaller. Finally, the fluid exiting the turbines with a lower flow rate will affect the condensing pressure (i.e. *P_condenser_adim*).

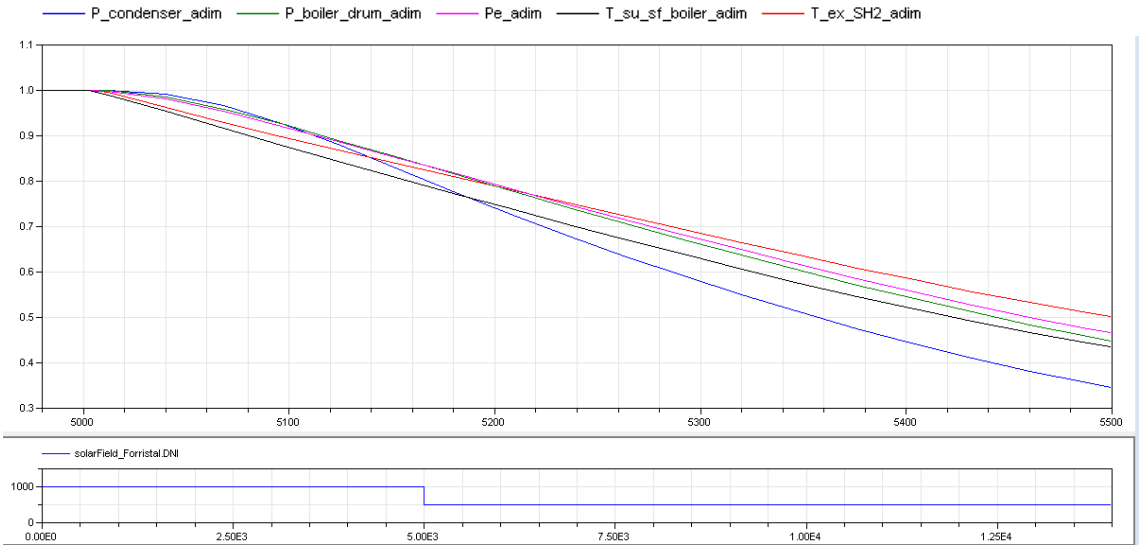

Figure 68: Zoom of Figure 67 and irradiation plot

After a certain simulation time, the "proximity" criteria becomes negligible, and the response time mainly depends on the "natural" dynamics of the system. The

condenser pressure, for example, is largely independent of the rest of the cycle, which explains why it is the fastest to decrease to its new steady-state value. On the contrary, the temperature of the oil, which was obviously the first effect of varying the solar irradiation data, continues changing in a slower pace. The boiler's pressure and the electrical power remain closely related one to another, i.e. as soon as the first one decreases (leading to a lower flow rate), the second one follows it.

Comparison with a finite volume model

In order to assess the computational efficiency the model, a comparison with another model is performed. For a fair comparison, the two models should refer to the same system. However, building such a model with a traditional library is very time consuming and could not be performed during this thesis. The comparison is only a rough, order-of-magnitude comparison with a similar model from the ThermoPower library. The selected model is the *SteamPlant_Sim1*, from the ThermoPower 2.1 library: a steam cycle model made of a 3-pressure level boiler using 1D discretization, a turbines section and a control system. Although the boiler design is slightly more complex than the one proposed in this work, there is no modeling of the heat source (in this work: the solar field), no preheater, no by-pass, and the condenser is modeled by a prescribed pressure. The ThermoPower model is therefore simpler than that proposed in this work.

The comparison is made on the computation time for one grid interval. After a successfully simulation of 8000s, this time is about 44.6 mili-seconds for the *Simulation 1* model, and about 238 mili-seconds for the ThermoPower model. The lumped model is therefore about 5 times faster than the finite volume model. Nevertheless, a more extensive comparison would be needed to confirm this.

6.2 Simulation 2: Varying the working fluid flow rate in the preheater

The second simulation consists in analyzing the response of the cycle when varying the mass flow rate of the extraction after the super-heated section going to the preheater (see Figure 60). The valve opening after the preheater (working fluid side) is used to control the mass flow rate of this extraction: a step up from an opening of 1 to 14 is applied at time 4000s. As shown in Figure 69, this opening entails a significant mass flow increase, up to 0.4 kg/s.

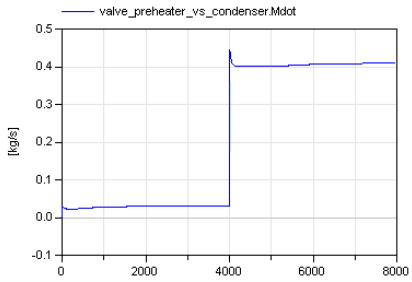

Figure 69: Mass flow rate (wf) in the preheater

When increasing the mass flow rate through the preheater, less mass flow rate is sent to the turbines, and therefore less electrical power is produced. As shown in Figure 70 and Figure 71, an immediate effect appears on the efficiency of the cycle and global (i.e. it considerably decreases in a short period of time). However, there is a secondary effect due to the fact that the secondary fluid has been more heated in the preheater (which tends to increase the efficiency). Nevertheless, this effect does not appear until the flow has gone through all the cycle. Therefore, a first immediate large drop of the instantaneous efficiency is stated, followed by a moderate increase after some time. The global balance is that the efficiency decreases when opening that valve.

Figure 70: Instantaneous efficiency of the cycle

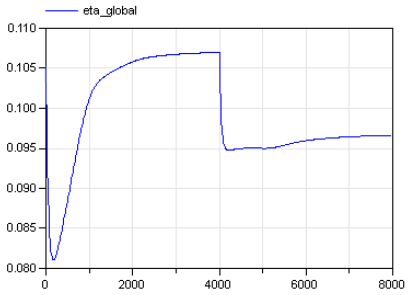

Figure 71: Efficiency of the overall plant

As shown in Figure 72, the effects on the boiler pressure follow the same trend. This effect can be expected since diverting the turbine inlet flow will inevitably reduce the efficiency, even if this flow is used to preheat the liquid. In practice, this flow is used as a nozzle-ejector vacuum pump for the condenser, in order to remove the non-condensable gases. However, this component is not modeled in the present work.

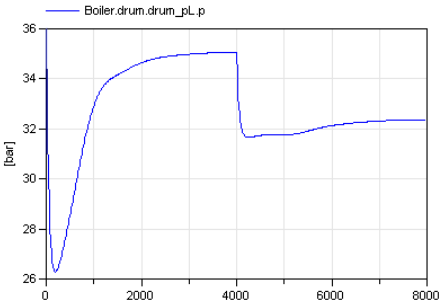

Figure 72: Pressure in the boiler

6.3 Simulation 3: Changing the position of the steam extraction

The third simulation consists in changing the location of the steam extraction to the preheater. The one before the first turbine is suppressed, and is moved between the high and low pressure turbines, as shown in Figure 73. With this configuration and according to steam cycle theory, a proper flow rate of the extraction to the preheater could increase the efficiency of the steam cycle. In comparison with the previous configuration, the main difference is that this portion of steam is now expanded in the high pressure turbine before being used for preheating. Therefore, more electrical power is produced.

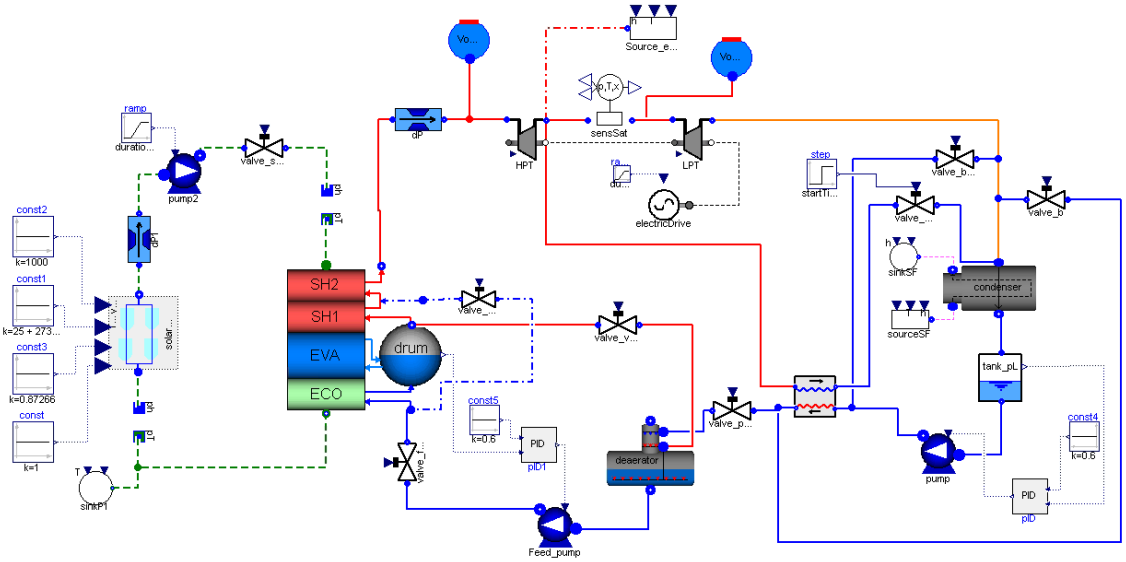

Figure 73: New configuration of the model

In the simulation, the opening of the valve after the preheater (working fluid side) is controlled externally with a ramp in order to regulate the mass flow rate of the extraction. The ramp starts closing the valve at 1000s and ends at 3500s, in order to decrease the mass flow rate until it is very low (but not null), as it is shown in Figure 74. The ramp speed is very low in order to avoid dynamic effects and evaluate the cycle efficiency in quasi-steady-state.

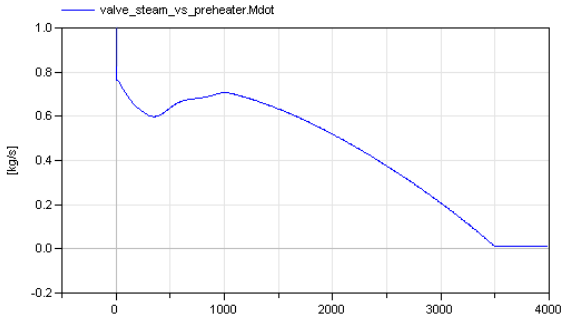

Figure 74: Mass flow rate in the valve

Figure 75 shows the vapor quality at the end of the preheater (in the last cell) of the working fluid. It can logically be seen that at lower flow rates, the working fluid gets more condensed (it starts with an 80% vapor quality and it ends sub-cooled).

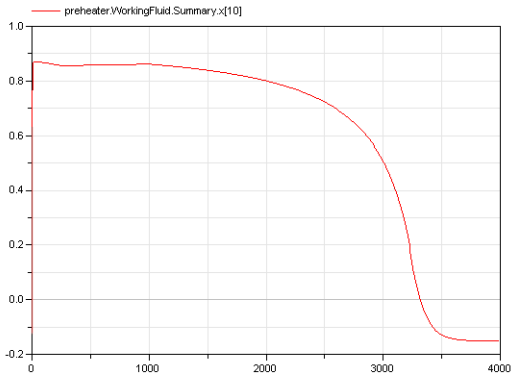

Figure 75: Vapor quality

As shown in Figure 76, the efficiency of the cycle presents a maximum. Comparing Figure 75 with Figure 76, it can be seen that this maximum is reached when the working fluid is condensed at the outlet of the preheater: if the flow rate is too high, the extracted fraction is not fully condensed, which is a waste of energy, whereas if the flow is too small, the regenerative effect of the extraction is decreased, which reduces the cycle efficiency as well.

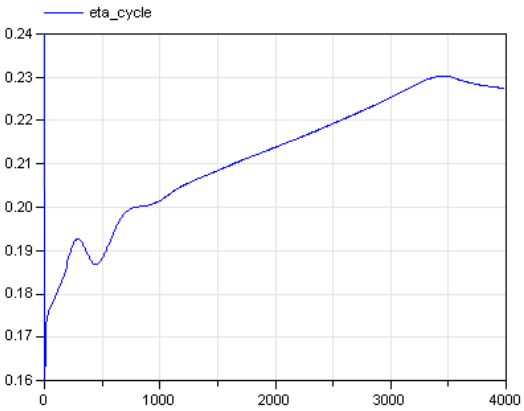

Figure 76: Efficiency of the steam cycle

In summary, this simulation shows that the model indeed predicts an efficiency increase due to steam extraction and preheating, but it also shows that a proper control of the extracted flow rate should be implemented.

6.4 Simulation 4: Varying the mass flow rate in the evaporator

The fourth simulation consists in analyzing the response of the cycle when varying the flow rate in the evaporator. The flow that enters the latter is pumped from the boiler

drum. Therefore, an external command for the pump frequency is added, in order to control its speed. As shown in Figure 77, the mass flow rate is completely defined by the step, which changes from 20Hz to 50Hz at 4000s.

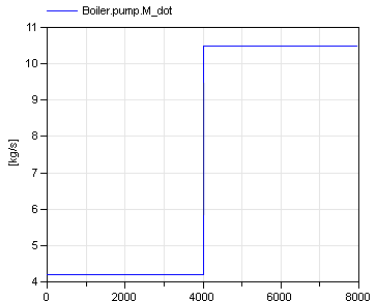

Figure 77: Mass flow rate pumped to the evaporator

As expected, increasing the mass flow rate in the evaporator leads to a lower vapor quality at the evaporator outlet, as shown in Figure 78. A too low frequency (such as 20Hz) is not suitable for the pump because the flow gets excessively evaporated and can cause choking in the boiler tubes, together with hot spots that can damage the boiler. A too high pump speed should also be avoided since it increases the pumping power and results in low vapor qualities, which do not correspond to the optimum heat transfer in the evaporator.

Figure 78: Real and nominal vapor quality at the evaporator outlet

However, in this simulation, due to the evaporator is modeled with a constant heat transfer coefficient (U), the gradient of temperature remains equal, and the heat transfer involved in it is constant too. Therefore, the variations on the mass flow rate of the evaporator do not influence the rest of the cycle (except the pump consumption). As shown in Figure 79 and Figure 80, the efficiency of the cycle and the pressure in the boiler are almost constant.

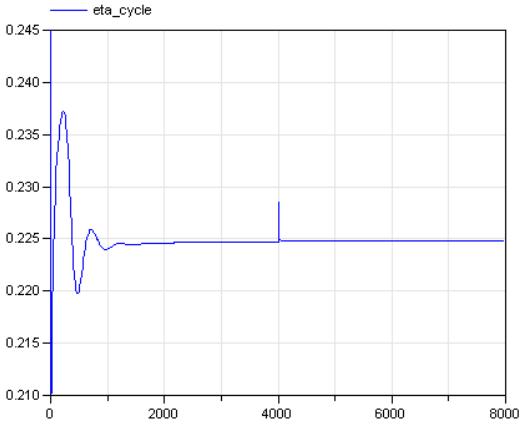

Figure 79: Efficiency of the steam cycle

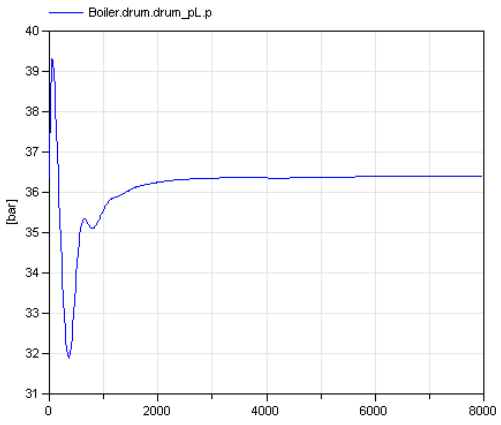

Figure 80: Pressure in the boiler

In reality, the heat transfer coefficient is not constant during evaporation or condensation. If the modeled heat transfer coefficient was a function of the mass flow rate and vapor quality, it is very likely that an optimum mass flow rate would be computed, which would require a proper control of the evaporator pump.

Chapter 7

Conclusions and perspectives

Library of lumped-parameter dynamic models

The main goal of this work was to design a library of semi-empirical dynamic models that are simplified but also physically meaningful, and whose main characteristics are robustness and computational efficiency.

The selected approach to achieve the above objective was to simplify the different component models to get rid of non-essential effects for the purpose of the simulation.

The main characteristic of the library is the LMTD formulation for the heat exchanger models. This formulation, which is originally only valid for steady-state, has been extended to transient simulation by dividing the heat transfer problem in two and adding a thermal mass. The single-phase heat transfer function *LMTD_robust* has increased significantly the robustness of the model. The model does not take into account heterogeneous flow (i.e. a slip factor between the vapor and liquid phases) or mass accumulation within the heat exchanger.

Linearizing the valve equations has also been very useful for this work, because it has significantly simplified the differential equation system. However, this does not allow accurately computing the valve pressure drop or flow reversals.

The computation efficiency of the condenser model has been proven during this work: the model rapidly adapts itself when transient conditions are involved. The working fluid is modeled in a simplified manner, assuming a constant heat transfer coefficient. This simplifies the real heat transfer phenomenon, but again significantly improves the robustness and computation efficiency of the model compared to finite volume models. It should be reminded though, that it is only valid when the super-heating and sub-cooling parts are practically inexistent, and that it is not sufficient to represent a physical condenser because it does not consider the condensed steam flow collected at the bottom of the condenser.

The preheater is the only two-phase finite volume model in the overall cycle model. Despite being discretized, a constant mass flow rate has been assumed to simplify the system. It would be interesting to change this model for a moving boundaries heat exchanger model, which is about three times faster than a discretized model, according to (Bendapudi et al., 2008). However, this type of model is not already available in ThermoCycle.

The turbine component offers the possibility of modeling the turbine by the Stodola's law. Although the model does not consider any dynamics, it is suitable to dynamic simulation since rotor and thermal inertia are usually very fast in a turbine. Moreover, the original Stodola formulation has been modified to allow the solver to continue even if the exhaust pressure is higher than the inlet one. Connecting more than one turbine in series can lead to numerical problems. The newly developed *Volume* model turned out to significantly increase the robustness of the initialization process.

Finally, different simulations have shown the suitability of the model for control purposes (e.g. with the introduction of the PI controllers), for the cycle performance evaluation, and for the evaluation of the system dynamics. The performance indicators present realistic values, although they cannot be validated with experimental data at this state. The cycle response to different steps and ramps on the boundary conditions also present realistic trends. Finally, it could be shown, through the modification of the preheater configuration, that cycle improvements can easily be simulated with this model.

Future works

This thesis is a first proposal for more simple, but still physical dynamic models. However, it is very important to note that **it has not been possible to validate the proposed model in the scope of this work**. The main priority for future works will therefore be the validation of these models, either with experimental data, or with other well-known and more detailed models.

It would also be interesting to define rules to properly set and calibrate the lumped parameters of the different models. As an example, the unique thermal mass of the proposed heat exchanger model should account for the thermal mass of the wall, but also for that of the primary and secondary fluids. Proper calibration rules should therefore be defined for that purpose.

Regarding the *LMTD_robust* method, a validation over typical conditions for various types of power plants should also be performed to evaluate the error in the case where the temperature profiles cross each other. It would also be great to improve the

function itself to make it C1-continuous, which would also increase the computational efficiency, especially when operating with low pinch point differences.

For the evaporator (i.e. two-phase model), a good implementation would be to add a heat transfer model that makes the heat transfer coefficient depending on, for example, the mass flow rate. It is an important aspect to consider when regulating the mass flow rate of the evaporator according to the requirements of the boiler system.

It should be also interesting to design a more complex control of the plant that involves the whole system and not only controls the levels of the drums. Moreover, the steam jet ejector vacuum pump present in the CHP plant could be implemented in order to model the extraction of air inside the condenser.

Summarizing, the developed lumped models are robust and computationally efficient and the convergence of the Newton Solver is therefore ensured. They seem to be significantly faster than the traditional finite volume models, although a more extensive comparison would be needed to confirm this. Nevertheless, they are limited to high level simulations and do not allow to compute detailed physical phenomena. They present a very interesting potential for future development and use, but more work is needed to demonstrate their validity and their limitations.

Bibliography

ARI (2014). Datasheets of the CHP plant in Sart-Tilman (Confidential).

Bell, I.H., Wronski, J., Quoilin, S., and Lemort, V. (2014). Pure and pseudo-pure fluid thermophysical property evaluation and the open-source thermophysical property library Coolprop. Ind. Eng. Chem. Res. *53*, 2498–2508.

Bendapudi, S., Braun, J.E., and Groll, E.A. (2008). A comparison of moving-boundary and finite-volume formulations for transients in centrifugal chillers. Int. J. Refrig. *31*, 1437–1452.

Bonilla, J., Yebra, L.J., and Dormido, S. (2011). A heuristic method to minimise the chattering problem in dynamic mathematical two-phase flow models. Math. Comput. Model. *54*, 1549–1560.

Casella, F., and Leva, A. (2003). Modelica open library for power plant simulation: design and experimental validation. In Proceeding of the 2003 Modelica Conference, Linkoping, Sweden,.

Casella, F., and Leva, A. (2009). The ThermoPower Library.

Casella, F., van Putten, J.G., and Colonna, P. (2007). Dynamic simulation of a biomass-fired steam power plant: a comparison between causal and a-causal modular modeling. In ASME 2007 International Mechanical Engineering Congress and Exposition, (American Society of Mechanical Engineers), pp. 205–216.

Colonna, P., and Van der Stelt, T.P. (2004). FluidProp: a program for the estimation of thermo physical properties of fluids. Energy Technol. Sect. Delft Univ. Technol. Delft Neth. Httpwww FluidProp Com.

Espinosa, N., Gil-Roman, I., Didiot, D., Lemort, V., Lombard, B., and Quoilin, S. (2011). Transient organic Rankine cycle modelling for waste heat recovery on a truck. In 24th International Conference on Efficiency, Cost, Optimization, Simulation and Environmental Impact of Energy Systems,.

Forristall, R.E. (2003). Heat transfer analysis and modeling of a parabolic trough solar receiver implemented in engineering equation solver (National Renewable Energy Laboratory).

Franke, R., Casella, F., Otter, M., Sielemann, M., Elmqvist, H., Mattson, S.E., and Olsson, H. (2009). Stream Connectors-An Extension of Modelica for Device-Oriented Modeling of Convective Transport Phenomena. In Proceedings of the 7th International Modelica Conference, (Linköping University Electronic Press), pp. 108–121.

Fritzson, P. (2010). Principles of object-oriented modeling and simulation with Modelica 2.1 (John Wiley & Sons).

Granulenergie (2014). http://www.granulenergie.fr/pour-tout-savoir/portraits-dutilisateurs/des-pellets-de-bois-pour-chauffer-le-campus-du-sart-tilman-a-liege.

Herrmann, U., Geyer, M., and Kistner, R. (2002). The AndaSol Project (FLABEG Solar International GmbH, Solar Millennium AG).

International Energy Agency (2010). Technology Roadmap: Concentrating Solar Power (OECD/IEA).

International Energy Agency (2011). Solar Energy Perspectives.

Jensen, J.M. (2003). Dynamic Modeling of Thermo-fluid Systems: With Focus on Evaporators for Refrigeration (Department of Mechanical Engineering, Technical University of Denmark).

Kakaç, S., Liu, H., and Pramuanjaroenkij, A. (1997). Heat Exchangers: Selection, Rating, and Thermal Design, Second Edition (Taylor & Francis).

Llorente García, I., Álvarez, J.L., and Blanco, D. (2011). Performance model for parabolic trough solar thermal power plants with thermal storage: comparison to operating plant data. Sol. Energy *85*, 2443–2460.

Lu, S. (1999). Dynamic modelling and simulation of power plant systems. Proc. Inst. Mech. Eng. Part J. Power Energy *213*, 7–22.

Manenti, F., and Ravaghi-Ardebili, Z. (2013). Dynamic simulation of concentrating solar power plant and two-tanks direct thermal energy storage. Energy *55*, 89–97.

Nellis, G., and Klein, S. (2009). Heat Transfer (Cambridge University Press).

Powell, K.M., and Edgar, T.F. (2012). Modeling and control of a solar thermal power plant with thermal energy storage. Chem. Eng. Sci. *71*, 138–145.

Quoilin, S. (2007). Les Centrales Solaires à Concentration.

Quoilin, S. (2011). Sustainable Energy Conversion Through the Use of Organic Rankine Cycles for Waste Heat Recovery and Solar Applications. University of Liège (Belgium.

Quoilin, S., Orosz, M., Hemond, H., and Lemort, V. (2011a). Performance and design optimization of a low-cost solar organic Rankine cycle for remote power generation. Sol. Energy *85*, 955–966.

Quoilin, S., Aumann, R., Grill, A., Schuster, A., Lemort, V., and Spliethoff, H. (2011b). Dynamic modeling and optimal control strategy of waste heat recovery Organic Rankine Cycles. Appl. Energy *88*, 2183–2190.

Quoilin, S., Bell, I., Desideri, A., Dewallef, P., and Lemort, V. (2014a). Methods to increase the robustness of finite-volume flow models in thermodynamic systems. Energies *7*, 1621–1640.

Quoilin, S., Desideri, A., Wronski, J., Bell, I., and Lemort, V. (2014b). ThermoCycle: A Modelica library for the simulation of thermodynamic systems. In 10th International Modelica Conference,.

Renewable Energy Policy Network for the 21st Century (2013). Renewables 2013 Global Status Report (REN21).

Ritcher, C., and Casella, F. (2008). ExternalMedia: A library for easy re-use of external fluid property code in Modelica. Proceeding 6th Int. Model. Conf.

Sartor, K., Quoilin, S., and Dewallef, P. (2014). Simulation and optimization of a CHP biomass plant and district heating network. Appl. Energy.

SolarPACES (2014). http://www.solarpaces.org/.

SOLUTIA (2014). THERMINOL VP-1. Vapour Phase. Liquid Phase. Heat Transfer Fluid. 12^{o}C to 100^{o}C.

ThermoCycle (2014). http://www.thermocycle.net/.

Tummescheit, H. (2002). Design and implementation of object-oriented model libraries using modelica. Lund University.

Tummescheit, H., Eborn, J., and Wagner, F. (2000). Development of a Modelica base library for modeling of thermo-hydraulic systems. In Modelica Workshop 2000 Proceedings, pp. 41–51.